MIPT/FALT-1999-010

# RECEPTIVITY OF HYPERSONIC BOUNDARY LAYER TO WALL DISTURBANCES

Alexander V. Fedorov

Moscow Institute of Physics and Technology
16 Gagarin Street, Zhukovki, Moscow Region, 140160
Russia



European Office of Aerospace Research and Development
Project SPC-98-4036
Contract F61775-98-WE039



May 1999

# REPORT DOCUMENTATION PAGE

Form Approved OMB No. 0704-0188



| 1. AGENCY USE ONLY (Leave blank) | 2. REPORT DATE | 3. REPORT TYPE AND DATES COVERED |
|---|---|---|
| | May 1999 | Final Report |

4. TITLE AND SUBTITLE

Receptivity of Hypersonic Non-Gradient Boundary Layer to Wall Disturbances

5. FUNDING NUMBERS

F61775-98-WE039

6. AUTHOR(S)

Dr. Alexander Fedorov

7. PERFORMING ORGANIZATION NAME(S) AND ADDRESS(ES)

Moscow Inst. of Physics and Technology
16 Gagarin St,
Zhukovsky 140160
Russia

8. PERFORMING ORGANIZATION REPORT NUMBER

N/A

9. SPONSORING/MONITORING AGENCY NAME(S) AND ADDRESS(ES)

EOARD
PSC 802 BOX 14
FPO 09499-0200

10. SPONSORING/MONITORING AGENCY REPORT NUMBER

SPC 98-4036

11. SUPPLEMENTARY NOTES

12a. DISTRIBUTION/AVAILABILITY STATEMENT

Approved for public release; distribution is unlimited.

12b. DISTRIBUTION CODE

A

13. ABSTRACT (Maximum 200 words)

This report results from a contract tasking Moscow Inst. of Physics and Technology as follows: The contractor will perform theoretical analysis of the hypersonic boundary-layer receptivity as outlined in his proposal originally submitted in Aug '97 and amended in Feb '98.

14. SUBJECT TERMS

EOARD, Boundary Layer transition, Hypersonic Flow

15. NUMBER OF PAGES

75

16. PRICE CODE

N/A

| 17. SECURITY CLASSIFICATION OF REPORT | 18. SECURITY CLASSIFICATION OF THIS PAGE | 19. SECURITY CLASSIFICATION OF ABSTRACT | 20. LIMITATION OF ABSTRACT |
|---|---|---|---|
| UNCLASSIFIED | UNCLASSIFIED | UNCLASSIFIED | UL |

## Abstract

Theoretical analysis of hypersonic boundary-layer receptivity to wall disturbances is conducted using a combination of asymptotic and numerical methods. Excitation of the second-mode waves by distributed and local forcing on the flat plate surface is studied under adiabatic and cooled wall conditions. Analysis addresses receptivity to wall vibrations, periodic suction-blowing through a hole or slot, and temperature disturbances. A strong excitation occurs in local regions where forcing is in resonance with normal waves. It is revealed that the receptivity function tends to infinity as the resonance point tends to the branch point of discrete spectrum that is typical for the cooled wall case. Asymptotic analysis resolves this singularity and provides maximal receptivity levels in the branch-point vicinity. Analytical results are integrated into the computational module providing fast estimates of receptivity levels for different types and shapes of wall forcing. Numerical results indicate extremely high receptivity to vibrations and suction-blowing near the lower neutral branch. Critical amplitudes of local and distributed vibrations are estimated for bypass of the linear stability phase. The theoretical model can be used to predict initial amplitudes of unstable waves in active (ascending) flights accompanied by skin vibrations.

## Table of contents

## Acknowledgments

The author wishes to express his sincere thanks to Dr. Roger Kimmel for useful discussions of results. Help in asymptotic analysis provided by Dr. Andrew Khokhlov is gratefully acknowledged.

The work was sponsored by the European Office of Aerospace Research and Development under Contract F61775-98-WE039. The author thankfully acknowledges the support of Dr. Charbel Raffoul.

## Nomenclature

### *Latin symbols*

| | |
|---|---|
| $\vec{A}_k$ | eigenfunction vector (direct problem) |
| $\vec{B}_k$ | eigenfunction vector (conjugate problem) |
| $c$ | phase speed |
| $F = \omega^* \nu_e^* / U_e^{*2}$ | frequency parameter |
| $G$ | receptivity function |
| $g$ | forcing shape-function |
| $L$ | streamwise scale |
| $M$ | Mach number |
| $N$ | amplification factor |
| $p$ | pressure disturbance |
| $Q$ | mass-flux disturbance |
| $q$ | receptivity factor |
| $R = \sqrt{U_e^* x^* / \nu_e^*}$ | Reynolds number |
| $t$ | time |
| $T$ | mean flow temperature |
| $U$ | mean flow streamwise velocity |
| $V$ | mean flow vertical velocity |
| $u, v, w$ | velocity disturbance |
| $x, y, z$ | Cartesian coordinates |
| $x_1 = x^* / L = \varepsilon x$ | slow streamwise variable |

### *Greek symbols*

| | |
|---|---|
| $\alpha, \beta$ | wave-vector components in x- and z-direction respectively |
| $\varepsilon = \delta / L$ | small parameter |
| $\Delta$ | delta function |
| $\delta = \sqrt{\nu_e^* L / U_e^*}$ | boundary layer thickness scale |
| $\nu$ | kinematic viscosity |

| | |
|---|---|
| $\rho(\alpha,\beta)$ | Fourier component of the shape-function $g(x',z')$ |
| $\omega$ | angular frequency |
| $\theta$ | temperature disturbance |
| $\bar{\Psi}$ | disturbance vector-function |
| $\bar{F}(x,y)$ | disturbance amplitude vector-function |

### *Subscripts*

| | |
|---|---|
| 0 | resonance point |
| *ad* | adiabatic wall |
| *b* | branch point |
| *e* | upper boundary-layer edge |
| *i* | imaginary part |
| *r* | real part |
| *s* | suction-blowing |
| *vib* | vibrations |
| *w* | wall |
| $\theta$ | temperature perturbation |

### *Superscripts*

| | |
|---|---|
| bar | complex conjugate value |
| asterisk | dimensional value |

### *Abbreviations*

| | |
|---|---|
| PSE | parabolized stability equations |
| Im | imaginary part |
| Re | real part |

## List of figures

# 1. Introduction

In hypersonic flights and quiet wind tunnels, freestream perturbations and body-induced disturbances are normally small. In this case, the transition process can be treated as an initial boundary value problem, which comprises excitation of unstable boundary-layer modes (receptivity problem), their downstream amplification (linear stability problem) and nonlinear breakdown to turbulence [1, 2]. Transition prediction technology is usually based on the $e^N$-method [3-5], which considers only the linear phase of instability growth. All other physics including receptivity and nonlinear breakdown is incorporated into the value $N$, which is colibrated for a particular set of experimental data. The finite amplitude method including receptivity, instability amplification, and an amplitude criterion for transition onset can avoid many shortcomings of the $e^N$-method. Recent codes based on the parabolized stability equations (PSE) can predict the instability evolution and capture the initial phase of nonlinear breakdown [6-8]. However the PSE codes require initial distributions of the disturbance amplitude as an input, which should be supplied by receptivity theory.

Despite of a good progress in experimental studies of hypersonic stability [9], we found only few papers relevant to experiments on hypersonic receptivity [10, 11]. Kendall [10] measured correlation between the freestream and boundary-layer disturbances in the Mach number range 1.6-5.6, and found that the correlation coefficient is growing with the Mach number. Experimental data obtained on a flat plate at Mach 4.5 are in a good agreement with the forcing theory of Mack [12]. However Mack noted that the major difficulty in the use of the forcing theory is that force disturbances are distinct from free disturbances, and the process by which the former becomes the latter is unknown. Maslov, Shiplyuk, Sidorenko and Arnal [11] studied the flat-plate leading edge receptivity to acoustic disturbances in the Mach 6 wind tunnel. Acoustic field was generated by a point source and plane source. It was found that the leading edge receptivity depends on the acoustic wave inclination angle $\chi$. Maximum receptivity was observed at $\chi \approx 60^\circ$. The receptivity coefficient for two-dimensional acoustic waves with the phase speed $c = 1 - 1/M_e$ was much larger than that measured for three-dimensional acoustic waves generated by the point

source. These observations are consistent with the theoretical results of Fedorov and Khokhlov [13].

Only few theoretical studies have been addressed hypersonic receptivity problem. Fedorov and Khokhlov [13] analyzed receptivity on the sharp leading edge of a flat plate to external disturbances including sound waves, entropy and vortical waves as well as leading-edge vibrations. They showed that freestream noise and/or vortical disturbances induce a local acoustic source on the leading edge. This source generates acoustic waves, which are synchronized with boundary-layer normal modes (the first and second modes according to Mack's classification). That causes a strong excitation of unstable normal waves by freestream disturbances through the mechanism, which is qualitatively different from that observed at subsonic speeds [14-19]. Zhong [20] performed direct numerical simulation of the parabolic leading-edge receptivity to freestream sound in a hypersonic flow. In his calculations, shock-layer modes and unstable boundary-layer modes were detected between a bow shock and body surface. Fedorov [21] showed that external vorticity and entropy disturbances can effectively generate the second mode near the lower neutral branch. In this region, the first and second mode waves can be synchronized with entropy/vorticity waves of the phase speed $c = 1$. In the synchronism region, entropy/vorticity disturbances are partially swallowed by the boundary layer and excite instability. This mechanism can compete with the leading-edge receptivity in cases of conical configurations such as a sharp cone.

Another important type of disturbances is associated with body-induced perturbations. In active flights, propulsion system generates vibrations of the vehicle skin. These vibrations can propagate upstream and excite the boundary-layer instability on the forebody surface. Skuratov, Fedorov and Shogin [22] published transition data obtained on a $7.5^\circ$ half-angle sharp cone installed on the rocket nose. Transition loci were measured during ascending flights in the local Mach number range $2.5-4$ at wall temperature ratios $T_w / T_{ad} = 0.2-0.8$. Transition onset points were close to those obtained in conventional (noisy) wind tunnels. Such an early transition seemed to be due to vibrations of the cone surface. Another source of disturbances is associated with gaps and slots between elements of the thermal protection system.

They may work as resonators, which induce periodic suction-blowing on the body surface. These perturbations can also generate unstable modes in the boundary layer.

Theoretical and experimental studies of the boundary-layer receptivity to body-induced perturbations have been performed for subsonic flows. It was found that the boundary layer is extremely sensitive to wall perturbations to be in resonance with Tollmien-Schlichting waves. For example, the theoretical analysis [23] and the wind-tunnel experiment [24] showed that two-dimensional vibrations of 5 microns amplitude (about 1% of the boundary-layer thickness) generate the TS waves with the initial amplitude $A_{in} \approx 0.1\%$. Assuming that nonlinear breakdown occurs at the critical amplitude $A_{cr} \approx 1\%$, we obtain that the amplification factor is $N = \ln(A_{cr} / A_{in}) \approx 2.3$. This value is much less than the empirical value $N \approx 10$ typical for "quiet" conditions. Similar conclusion has been made regarding periodic suction-blowing induced through a two-dimensional slot in subsonic flat plate [25]. These findings lead to the assumption that hypersonic boundary layers may be also very receptive to wall perturbations.

In this report, we perform theoretical analysis of hypersonic boundary-layer receptivity to wall disturbances. We consider excitation of the second-mode waves by distributed and local forcing on a flat plate. In Section 2 we formulate the problem, analyze disturbance field in the case of resonance between the second-mode wave and distributed wall forcing. Then we consider receptivity to local forcing produced by a vibrator, periodic suction-blowing through a slot or hole, and temperature perturbations induced by a heating element. In Section 3 we describe computational algorithm providing the receptivity function and discuss numerical results for adiabatic and cooled plate cases. We show that the receptivity function tends to infinity as the resonance point tends to the branch point of the discrete spectrum. Receptivity to wall forcing in the branch-point vicinity is analyzed in Section 4. Critical amplitudes of wall vibrations providing bypass of the linear stability phase are estimated in Sections 5 for local and distributed forcing. In Section 6, we conclude the report and discuss future effort.

## 2. Receptivity to wall perturbations in the case of a simple discrete spectrum

In this section, we analyze the disturbance field generated by wall perturbations in the case of a simple discrete spectrum; *i.e.* eigenvalues of the boundary-layer modes are assumed to be different. Under this condition, analysis of hypersonic boundary-layer receptivity to wall forcing can be performed using the theoretical model of [23, 25, 26] developed for subsonic boundary layers.

### *2.1 Problem formulation for distributed forcing*

We consider a two-dimensional laminar boundary layer of perfect gas on a hypersonic flat plate schematically shown in Fig. 1. It is assumed that the global streamwise length $L$ is much larger than the boundary layer thickness scale $\delta = \sqrt{\nu_e^* L / U_e^*}$; *i.e.* the ratio $\varepsilon = \delta / L$ is small. This is equivalent to the assumption that the Reynolds number $R_L = \sqrt{U_e^* L / \nu_e^*} = \varepsilon^{-1}$ is large. The longitudinal $x^*$, normal $y^*$, transversal $z^*$ coordinates and time $t^*$ are made nondimensional using $\delta$ and $U_e^*$ as

$$(x, y, z) = (x^*, y^*, z^*) / \delta \,,\; t = t^* U_e^* / \delta \,.$$

We introduce the slow variable $x_1 = x^* / L = \varepsilon x$ and specify the nondimensional mean-flow velocity components $(U, V)$ and temperature $T$ as

$$U \equiv U^* / U_e^* = U(x_1, y),\; V \equiv V^* / U_e^* = \varepsilon V_0(x_1, y),\; T \equiv T^* / T_e^* = T(x_1, y). \qquad (2.1)$$

Distributed perturbations of velocity $(u, v, w)$, pressure $p$ and temperature $\theta$ are induced by vibrations or any other forcing on the body surface. Wall perturbations are represented in the traveling-wave form

$$(u, v, w, \theta) = (\varphi_1, \varphi_2, \varphi_3, \varphi_4) \exp(i\alpha x + i\beta z - i\omega t) \text{ at } y = 0, \qquad (2.2)$$

where $\alpha$ and $\beta$ are wavenumber components; $\omega$ is angular frequency. The forcing amplitude is assumed to be small and the following analysis is performed using a linear theory of small perturbations. The flow disturbance is described by the vector function

$$\vec{\Psi} = (u, \frac{\partial u}{\partial y}, v, p, \theta, \frac{\partial \theta}{\partial y}, w, \frac{\partial w}{\partial y})^T, \tag{2.3}$$

$$\vec{\Psi}(x,y,z,t) = \vec{F}(x,y)\exp(i\beta z - i\omega t). \tag{2.4}$$

The amplitude function $\vec{F}(x,y)$ satisfies a system of partial differential equations resulted from Fourier transform of linearized Navier-Stokes equations with respect to time and $z$-coordinate. These equations can be written in the matrix-operator form

$$H(y, \partial_y, x_1, \varepsilon\partial_{x_1}, \omega, \beta)\vec{F} = 0. \tag{2.5}$$

Boundary conditions are specified as

$$(F_1, F_3, F_5, F_7) = (\varphi_1, \varphi_2, \varphi_3, \varphi_4)\exp(i\alpha x) \text{ at } y = 0, \tag{2.6}$$

$$|\vec{F}| < \infty \text{ at } y \to \infty. \tag{2.7}$$

As contrasted to a standard stability analysis, the problem (2.5)-(2.7) has non-homogeneous boundary conditions on the wall ($y = 0$) and describes the flow disturbance field, which, in general, includes forcing and normal waves generated by wall perturbations.

### *2.2 Non-resonance case*

We consider a partial solution of the problem (2.5)-(2.7) as a decomposition of the discrete modes $\vec{F}_k(x_1, y)$ with eigenvalues $\alpha_k(x_1, \beta, \omega)$ and the force term $\vec{F}_v(x_1, y)$ with the wavenumber $\alpha$. Then the disturbance amplitude is expressed in the form

$$\vec{F} = \sum_k (\vec{F}_{k0} + \varepsilon \vec{F}_{k1} + \cdots) \exp(i\varepsilon^{-1} S_k) + \vec{F}_v \exp(i\varepsilon^{-1} \alpha x_1), \tag{2.8}$$

$$S_k = \int_{x_{1s}}^{x_1} \alpha_k(x_1) dx_1 . \tag{2.9}$$

Substituting (2.8) into Eqs. (2.5)-(2.7) and grouping terms of the same order of magnitude with respect to $\varepsilon$ we obtain a sequence of problems for the amplitude functions $\vec{F}_{kj}(x_1, y)$, $j = 0, 1, \ldots$ In the first order approximation, we get the eigenvalue problem

$$\left(\frac{\partial}{\partial y} - H_0\right) \vec{F}_{k0} = 0, \tag{2.10a}$$

$$(F_{k0})_{1,3,5,7} = 0 \text{ at } y = 0, \tag{2.10b}$$

$$\left|\vec{F}_{k0}\right| \to 0 \text{ at } y \to \infty . \tag{2.10c}$$

Here the matrix $H_0$ has dimension $8 \times 8$; its elements depend on the mean-flow profiles $U(x_1, y)$ and $T(x_1, y)$, disturbance parameters $\alpha, \beta, \omega$ and Reynolds number $R = \sqrt{U_e^* x^* / \nu_e^*}$. Explicit form of the matrix $H_0$ is given in [26, 27]. Equations (2.10a)-(2.10c) form a standard linear stability equation system for locally parallel mean flows.

Forcing term $\vec{F}_v(x_1, y)$ is a solution of the non-homogeneous problem

$$\left(\frac{\partial}{\partial y} - H_0\right) \vec{F}_v = 0, \tag{2.11a}$$

$$(F_v)_{1,3,5,7} = \varphi_{1,2,3,4} \text{ at } y = 0, \tag{2.11b}$$

$$\left|\vec{F}_v\right| < \infty \text{ at } y \to \infty . \tag{2.11c}$$

If the forcing wavenumber $(\alpha, \beta)$ coincides with a wavenumber of continuous spectrum, then the body surface effectively generates acoustic, vortical or entropy waves. If $(\alpha, \beta)$

does not belong to the continuous spectrum, then the forcing disturbance decays exponentially as $y \to \infty$. Hereafter we analyze the latter case.

In the second order approximation, we obtain the non-homogeneous problem

$$\left(\frac{\partial}{\partial y} - H_0\right)\vec{F}_{k1} = -i\frac{\partial H_0}{\partial \alpha}\frac{\partial \vec{F}_{k0}}{\partial x_1} + H_1\vec{F}_{k0}, \tag{2.12a}$$

$$(F_{k1})_{1,3,5,7} = 0 \text{ at } y = 0, \tag{2.12b}$$

$$\left|\vec{F}_{k1}\right| \to 0 \text{ at } y \to \infty. \tag{2.12c}$$

An explicit form of the matrix $H_1$ is given in [26, 27]. Its elements depend on the mean-flow profile derivatives $\partial U / \partial x_1$, $\partial T / \partial x_1$ and vertical velocity $V_0$. This matrix is associated with nonparallel effects due to the boundary-layer downstream growth.

Solution of the eigenvalue problem (2.10) can be represented in the form

$$\vec{F}_{k0} = c_k(x_1)\vec{A}_k(x_1, y, \alpha_k), \tag{2.13}$$

where $\vec{A}_k$ is eigenfunction normalized by a certain condition. For example, the pressure disturbance amplitude is constant on the wall: $A_{k4}(x_1, 0, \alpha_k) = 1$. Problem (2.12) has a nontrivial solution if its right-hand side is orthogonal to the eigenfunction $\vec{B}_k(x_1, y, \alpha_k)$ of the conjugate problem. This leads to the following ordinary differential equation for the amplitude coefficient $c_k(x_1)$

$$i < \vec{B}_k, \frac{\partial H_0}{\partial \alpha}\vec{A}_k > \frac{dc_k}{dx_1} = [-i < \vec{B}_k, \frac{\partial H_0}{\partial \alpha}\frac{\partial \vec{A}_k}{\partial x_1} > + < \vec{B}_k, H_1\vec{A}_k >]c_k, \tag{2.14}$$

$$c_k(x_{1s}) = c_{ks}, \tag{2.15}$$

where the scalar product is defined as

$$< \vec{B}, \vec{A} >= \int_0^{\infty} \sum_{j=1}^{8} \overline{B}_j A_j \, dy \,. \tag{2.16}$$

Upper bar denotes complex conjugate values; the amplitude coefficient $c_k$ is assumed to be prescribed at some initial point $x_{1s}$.

If the interaction between normal modes is neglected, then Eq. (2.14) describes the normal wave propagation in a weakly nonparallel boundary layer. This approximation is valid in a region where eigenvalues are different; *i.e.* $\alpha_k(x_1) \neq \alpha_j(x_1)$ at $k \neq j$, and the forcing wavenumber $\alpha \neq \alpha_k$; *i.e.* in the absence of resonance between wall forcing and normal wave, receptivity is weak.

### *2.3 Resonance between forcing and normal waves*

We assume that the force wave is in resonance with a normal wave of discrete spectrum at some point $x_1 = x_{10}$; *i.e.* $\alpha \approx \alpha_n(x_{10}) \equiv \alpha_0$. We consider the case when the normal wave is unstable and the resonance point $x_{10}$ is close to the lower neutral branch. It is expected that the wall disturbance generates the normal wave in a local region near the resonance point. Downstream from this region, the normal-wave amplitude exponentially increases due to the boundary layer instability.

Flow scheme of resonant forcing is shown in Fig. 2. Analysis of Eqs. (2.5)-(2.7) indicates that a strong excitation occurs in a small region where $|x_1 - x_{10}| = O(\varepsilon^{1/2})$. We introduce the inner longitudinal variable as

$$\xi = \varepsilon^{-1/2}(x_1 - x_{10}) = O(1) \,. \tag{2.17}$$

In dimensional form, the resonance point is $x_0^* = L$, and the inner-region length is of the order of $l = L \cdot R_L^{-1/2} = \delta \cdot R_L^{1/2}$. This length is much larger than the boundary-layer thickness scale $\delta$ and much smaller than the distance $L$ from the plate leading edge to the resonance point.

We assume that the force wavenumber is $\alpha = \alpha_0 + \gamma\varepsilon^{1/2}$, where the real parameter $\gamma$ characterizes resonance detuning. Then the inner solution of Eqs. (2.5)-(2.7) is expressed in the form

$$\vec{F} = [\varepsilon^{-1/2} c(\xi)\vec{A}_0(y) + \vec{A}_v(\xi, y) + \ldots]\exp(i\varepsilon^{-1/2}\alpha_0\xi), \tag{2.18}$$

where $\vec{A}_0(y) = \vec{A}_n(x_{10}, y, \alpha_0)$ is the $n^{\text{th}}$-mode eigenfunction at the resonance point. Expanding the operator $H_0$ in the vicinity of $x = x_{10}$ we obtain the following inner problem for the force wave amplitude $\vec{A}_v$

$$\left(\frac{\partial}{\partial y} - H_0(x_{10}, \alpha_0)\right)\vec{A}_v = -i\frac{dc}{d\xi}\frac{\partial H_0}{\partial \alpha}(x_{10}, \alpha_0)\vec{A}_0 + c\xi\frac{\partial H_0}{\partial x_1}(x_{10}, \alpha_0)\vec{A}_0, \tag{2.19a}$$

$$(A_v)_{1,3,5,7} = \varphi_{1,2,3,4}(x_{10})\exp(i\gamma\xi) \text{ at } y = 0, \tag{2.19b}$$

$$\left|\vec{A}_v\right| \to 0 \text{ at } y \to \infty. \tag{2.19c}$$

Using a standard approach (see for example [28]) we can express the problem (2.19) in the form

$$\left(\frac{\partial}{\partial y} - H_0(x_{10}, \alpha_0)\right)\vec{A}_v = -i\frac{dc}{d\xi}\frac{\partial H_0}{\partial \alpha}(x_{10}, \alpha_0)\vec{A}_0 + c\xi\frac{\partial H_0}{\partial x_1}(x_{10}, \alpha_0)\vec{A}_0 + \Delta(y)\vec{\Phi}_0\exp(i\gamma\xi), \tag{2.20a}$$

$$(A_v)_{1,3,5,7} = 0 \text{ at } y = 0, \tag{2.20b}$$

$$\left|\vec{A}_v\right| \to 0 \text{ at } y \to \infty, \tag{2.20c}$$

$$\vec{\Phi}_0 = (\varphi_1(x_{10}), 0, \varphi_2(x_{10}), 0, \varphi_3(x_{10}), 0, \varphi_4(x_{10}), 0)^T, \tag{2.20d}$$

where $\Delta(y)$ is delta function. Problem (2.20) has a non-trivial solution, if its right-hand side is orthogonal to the eigenfunction $\vec{B}_0 = \vec{B}_n(x_{10}, y, \alpha_0)$ of the conjugate problem. This condition leads to the following equation for the amplitude coefficient $c(\xi)$

$$\frac{dc}{d\xi} - ib\xi c = q\exp(i\gamma\xi), \tag{2.21a}$$

$$b = \frac{d\alpha_n}{dx_1}(x_{10}), \tag{2.21b}$$

$$q = i\frac{(\vec{B}_0, \vec{\Phi}_0)_{y=0}}{< \vec{B}_0, \frac{\partial H_0}{\partial \alpha}(x_{10}, \alpha_0)\vec{A}_0 >}. \tag{2.21c}$$

If the normal wave has zero amplitude upstream from the resonance region, then the boundary condition for Eq. (2.21a) is specified as

$$c(\xi) \to 0 \text{ at } \xi \to -\infty. \tag{2.22}$$

Solution of the problem (2.21a), (2.22) is expressed in the form

$$c(\xi) = q\exp(ib\xi^2/2)\int_{-\infty}^{\xi}\exp\left(i\gamma s - \frac{ibs^2}{2}\right)ds. \tag{2.23}$$

In typical cases, the unstable mode eigenvalue satisfies the following conditions near the lower neutral branch:

$$d\,\mathrm{Re}(\alpha_n)/dx_1 > 0,\ d\,\mathrm{Im}(\alpha_n)/dx_1 < 0.$$

Then an asymptotic behavior of the amplitude coefficient $c(\xi)$ as $\xi \to +\infty$ is associated with the saddle point $s_* = \gamma / b$ and evaluated using the steepest descent method as

$$c(\xi) \to q\sqrt{\frac{2\pi i}{b}} \exp\left(\frac{i\gamma^2}{2b} + \frac{ib\xi^2}{2}\right) \text{ at } \xi \to +\infty . \tag{2.24}$$

Analyzing asymptotic trends of the outer solution $\tilde{F}_{n0}$ we conclude that its inner limit at $x_1 \to x_{10} + 0$ matches with the outer limit of the inner solution at $\xi \to +\infty$; *i.e.* in the resonance region, $x_1 - x_{10} = O(\varepsilon^{1/2})$, the force wave excites the unstable normal wave of the amplitude

$$\tilde{F}_n = \varepsilon^{-1/2} q\sqrt{\frac{2\pi i}{b}} \exp\left(\frac{i\gamma^2}{2b}\right) \bar{A}_n(x_1, y) \exp\left[ i\varepsilon^{-1} \int_{x_{10}}^{x_1} \alpha_n(x_1) dx_1 \right] \text{ for } x_1 > x_{10} . \tag{2.25}$$

This equation shows that the normal wave amplitude is proportional to $(L/\delta)^{1/2} = R_L^{1/2}$, whereas the resonant region length is $l = R_L^{1/2}\delta$. As the Reynolds number increases, nonparallel effects (which disturb the resonance condition) decrease and the relative length $l/\delta$ increases. In the parallel mean-flow limit, $R_L \to \infty$, the resonance region is infinitely large and the normal wave amplitude tends to infinity. In this case, the upper limit of disturbance amplitude is determined by nonlinear effects. Both nonlinear and nonparallel mechanisms of the resonance detuning can be observed simultaneously at sufficiently large Reynolds numbers and strong forcing. Note that the expression (2.25) is similar to that obtained by Tumin and Fedorov [23] for subsonic boundary layers using another approach.

### *2.4 Local forcing*

We consider a force disturbance, which is localized in a region comparable with the boundary layer thickness. This may be a vibrator, suction/blowing induced through a hole

(in three-dimensional case) or slot (in two-dimensional case), and temperature perturbations induced by a heating element. In the general case, the force shape is expressed in the vector form

$$\vec{\varphi} \equiv (u, v, \theta, w)^T\big|_{y=0} = g(x', z')\vec{\varphi}_0\,,\ x' = x - x_0 = \varepsilon^{-1}(x_1 - x_{10})\,,\ z' = z - z_0\,, \qquad (2.26)$$

where $\vec{\varphi}_0$ is force amplitude vector, which does not depend on the local coordinates $x'$ and $z'$. However this vector is a function of the force type and mean-flow characteristics at the central point $(x_0, z_0)$. Its explicit form will be given in Section 3.

The force shape vector-function is associated with the Fourier transform

$$\rho(\alpha, \beta) = \int_{-\infty}^{+\infty} dz' \int_{-\infty}^{+\infty} dx' g(x', z') \exp(-i\alpha x' - i\beta z'), \qquad (2.27)$$

and can be expressed as

$$\vec{\varphi} = \frac{\vec{\varphi}_0}{(2\pi)^2} \int_{-\infty}^{+\infty} d\beta \int_{-\infty}^{+\infty} \rho(\alpha, \beta) \exp(i\alpha x' + i\beta z') d\alpha =$$

$$\frac{\vec{\varphi}_0}{(2\pi)^2} \varepsilon^{1/2} e^{i\alpha_0 x'} \int_{-\infty}^{+\infty} d\beta \int_{-\infty}^{+\infty} \rho(\alpha_0 + \varepsilon^{1/2}\gamma, \beta) \exp(i\gamma\xi + i\beta z') d\gamma\,. \qquad (2.28)$$

For two-dimensional forcing of the shape $g(x')$, Equations (2.27) and (2.28) are reduced to the form

$$\rho(\alpha) = \int_{-\infty}^{+\infty} dx' g(x') \exp(-i\alpha x'), \qquad (2.29)$$

$$\vec{\varphi} = \frac{\vec{\varphi}_0}{2\pi} \int_{-\infty}^{+\infty} \rho(\alpha) \exp(i\alpha x') d\alpha = \frac{\vec{\varphi}_0}{2\pi} \varepsilon^{1/2} e^{i\alpha_0 x'} \int_{-\infty}^{+\infty} \rho(\alpha_0 + \varepsilon^{1/2}\gamma) \exp(i\gamma\xi) d\gamma\,. \qquad (2.30)$$

Using Eq. (2.25) we evaluate the normal-wave amplitude generated by force waves in the wavenumber range $(\alpha_0 + \varepsilon^{1/2}(\gamma + d\gamma), \beta + d\beta)$ as

$$d\vec{F}_n = \frac{q}{(2\pi)^2}\sqrt{\frac{2\pi i}{b}}\exp\left(\frac{i\gamma^2}{2b}\right)\rho(\alpha_0 + \varepsilon^{1/2}\gamma, \beta)\vec{A}_n(x', y; \beta)\exp\left(i\int_0^{x'}\alpha_n(x')dx'\right)e^{i\beta z'}d\gamma d\beta . \tag{2.31}$$

Integrating over $\gamma$ we get the following wave packet in the first order approximation

$$\vec{F}_n = \frac{1}{2\pi}\int_{-\infty}^{+\infty} q\rho(\alpha_0, \beta)\vec{A}_n(x', y; \beta)\exp\left(i\int_0^{x'}\alpha_n(x')dx' + i\beta z'\right)d\beta . \tag{2.32}$$

For two-dimensional forcing specified by Eqs. (2.29), (2.30), the normal wave amplitude is expressed as

$$\vec{F}_n = q\rho(\alpha_0)\vec{A}_n(x', y)\exp\left(i\int_0^{x'}\alpha_n(x')dx'\right). \tag{2.33}$$

According to Eq. (2.21c) the receptivity factor $q(x_{10}, \alpha_0)$ does not depend on the force shape $g(x', z')$. If this factor is calculated once and for all, then we can evaluate the normal wave amplitude induced by local forcing of any shape.

As contrasted to the case of distributed forcing (see Eq. (2.25)), local forcing generates the boundary-layer normal waves of a finite amplitude even in the parallel mean flow limit. This is due to the fact that only a small portion of the force spectrum, $(\alpha - \alpha_0) = O(\varepsilon^{1/2})$, is involved into the resonance mechanism. As $\varepsilon \to 0$, the resonant excitation increases proportionally to $\varepsilon^{-1/2}$, whereas the spectrum region is narrowed down proportionally to $\varepsilon^{1/2}$. Because both trends compensate each other, the normal-wave amplitude excited by local forcing tends to a finite value.

## 3. Numerical results

### *3.1 Computational algorithm for receptivity to local forcing*

Summarizing results of Section 2 we formulate the following algorithm for calculations of the normal-wave amplitude generated by local wall forcing:

1. Specify the function $\vec{\varphi}(x',z')$ defined by Eq. (2.26), where the vector $\vec{\varphi}_0$ depends on a forcing type. For vibrations, it is expressed as

$$\vec{\varphi}_0 = (U', i\omega, T', 0)^T_{y=0, x_1=x_{10}}, \tag{3.1}$$

where prime denotes the partial derifative $\partial / \partial y$. In this case, the force shape function $g(x',z')$ corresponds to the wall displacement amplitude.

For suction-blowing inducing a vertical velocity on the body surface, we obtain

$$\vec{\varphi}_0 = (0, 1, 0, 0)^T. \tag{3.2}$$

In this case, the function $g(x',z')$ determines the vertical velocity amplitude.

For temperature perturbations on the wall surface, we get

$$\vec{\varphi}_0 = (0, 0, 1, 0)^T. \tag{3.3}$$

In this case, the function $g(x',z')$ determines the surface temperature amplitude.

2. Solve direct and conjugate eigenvalue problems at the central point $x_1 = x_{10}$ of the force element and calculate the normal-wave eigenvalue $\alpha_0 = \alpha_n(x_{10}, \beta, \omega)$ and eigenfunctions $\vec{A}_0(y)$, $\vec{B}_0(y)$. This can be done using a standard stability code.

3. Calculate the receptivity factor $q(x_{10},\alpha_0,\beta,\omega)$ using Eq. (2.21c).

4. Evaluate the normal-wave amplitude $\bar{F}_n$ using Eq. (2.32) for three-dimensional forcing or Eq. (2.33) for two-dimensional forcing.

This algorithm was integrated in a computationally non-intensive module, which was coupled with a standard stability code. This module works as a black box and predicts initial amplitudes of unstable normal waves induced by wall forcing of prescribed shape.

### *3.2 Numerical results*

Calculations have been conducted for the Mack second-mode induced by a two-dimensional local forcing. For surface vibrations, the shape vector-function $\bar{\varphi}_0$ is determined from Eq. (3.1). The disturbance amplitude is characterized by the mass-flux perturbation evaluated at the point of its maximum: $y = y_m$. This quantity is expressed as

$$Q(x_{10},y_m) = \mid \rho(\alpha_0) \mid G_{vib}, \tag{3.4}$$

where Fourier component $\rho(\alpha)$ is determined from Eq. (2.29); the receptivity function for local vibrations is calculated using Eqs. (2.20d), (2.21c), (2.33) and (3.1) as

$$G_{vib}(x_{10},\alpha_0) = \left| Q_2(y_m,x_{10}) \frac{(U'B_{2,1} + i\omega B_{2,3} + T'B_{2,5})_{y=0,x_1=x_{10}}}{\left\langle \frac{\partial H_0}{\partial \alpha}(x_{10},\alpha_0)\vec{A}_2, \vec{B}_2 \right\rangle} \right|. \tag{3.5}$$

This function characterizes the mass-flux amplitude of the normal wave generated by a vibrator with the unit Fourier component $\rho(\alpha_0) = 1$; $Q_2(y_m,x_{10})$ is mass flux disturbance evaluated using the second-mode eigenfunction $\vec{A}_2$. For the boundary layer on a flat plate, the length scale is determined as $\delta = \sqrt{\nu_e^* x_0^* / U_e^*}$, and the Reynolds number is

$R=\sqrt{U_e^* x_0^* / \nu_e^*}$ . If the receptivity function $G_{vib}$ is known, then we can calculate the initial amplitude of the second-mode wave generated by a vibrator of arbitrary shape using Eqs. (3.4) and (2.33).

In a similar way, we evaluate receptivity to suction-blowing through a two-dimensional slot. The mass-flux perturbation is expressed in the form

$$Q(x_{10}, y_m) = |\rho(\alpha_0)| G_s, \tag{3.6}$$

where the receptivity function is determined from Eqs. (2.20d), (2.21c), (2.33) and (3.2) as

$$G_s(x_{10}, \alpha_0) = \left| Q_2(y_m, x_{10}) \frac{(B_{2,3})_{y=0, x_1=x_{10}}}{\left\langle \frac{\partial H_0}{\partial \alpha}(x_{10}, \alpha_0)\vec{A}_2, \vec{B}_2 \right\rangle} \right|. \tag{3.7}$$

The mass-flux disturbance excited by surface temperature perturbations is expressed in the form

$$Q(x_{10}, y_m) = |\rho(\alpha_0)| G_\theta, \tag{3.8}$$

where the receptivity function is determined from Eqs. (2.20d), (2.21c), (2.33) and (3.3) as

$$G_\theta(x_{10}, \alpha_0) = \left| Q_2(y_m, x_{10}) \frac{(B_{2,5})_{y=0, x_1=x_{10}}}{\left\langle \frac{\partial H_0}{\partial \alpha}(x_{10}, \alpha_0)\vec{A}_2, \vec{B}_2 \right\rangle} \right|. \tag{3.9}$$

**Case 1: Cooled wall**

Calculations of the receptivity functions $G_{vib}$, $G_s$ and $G_\theta$ versus the Reynolds number $R = \sqrt{U_e^* x_0^* / \nu_e^*}$ have been made for the following mean flow parameters: local Mach number $M_e = 5.95$, freestream temperature $T_e^* = 70.2578$ K, wall temperature ratio $T_w^* / T_e^* = 0.69539$ corresponding to the ratio $T_w / T_{ad} = 0.1$, specific heat ratio $c_p / c_v = 1.4$, Prandtl number Pr=0.72, second viscosity coefficient $k = 1.2$. Disturbance frequency parameter is $F = 10^{-4}$. As shown in [21] the discrete spectrum has a singular topology in this case. First and second modes have the branch points $R_{b1}$ and $R_{b2}$ located near the lower and upper neutral branch respectively. The first branch point is very close to the real axis of complex $R$-plane. The second branch point is slightly shifted from the real axis. In the vicinity of the branch points, the eigenvalue spectrum splits as shown in Figs. 3a and 3b (see also Figs. 14a of Ref. [21] for a conical boundary layer).

Figures 4a, 4b, 4c and 4d show the second-mode wave increment $-\alpha_i = -\mathrm{Im}\,\alpha_2(R)$ and the receptivity function $G_{vib}(R)$, $G_s(R)$ and $G_\theta(R)$ respectively. It is seen that the receptivity functions have a sharp peak at the Reynolds number $R \approx R_{b1}$. As shown in [21], the scalar product has the following trend near the branch point

$$\left\langle \frac{\partial H_0}{\partial \alpha} \vec{A}_n, \vec{B}_n \right\rangle \to 0 \text{ as } R \to R_{b1},\ n = 1,2. \tag{3.10}$$

According to Eqs. (3.5), (3.7) and (3.9) the receptivity functions tend to infinity as $R \to R_{b1}$. Second maximum of $G_{vib}(R)$, $G_s(R)$ and $G_\theta(R)$ is observed at the Reynolds number $R \approx 2500$, which is close to the second branch point $R_{b2}$. Because the point $R_{b2}$ is shifted to the complex $R$-plane this maximum is smaller and smoothed out. Comparing data in Figs. 4b-4d we conclude that receptivity to suction-blowing is several times higher than receptivity to vibrations. In turn, receptivity to vibrations is several times higher than receptivity to temperature perturbations.

Figures 5a, 5b, 5c and 5d show distributions of $-\alpha_i(R)$, $G_{vib}(R)$, $G_s(R)$ and $G_\theta(R)$ at various frequency parameters $F$. The highest peak of the receptivity function corresponds to Curve 3 at $F = 10^{-4}$. In this case, the first branch point $R_{b1}$ is very close to the real axis of the complex $R$-plane as shown in Fig. 6. For the frequency parameter $F < 10^{-4}$, the first branch point is located in the upper half of the complex $R$-plane (Points 4 and 5 in Fig. 6). As the Reynolds number increases along the real axis, this branch point is bypassed from the lower side. The first mode (with the phase speed behavior $c \to 1 + 1/M_e$ as $R$ decreases) becomes unstable. In this case, the phase speed crosses the ray $c = 1$ that causes discontinuity of the receptivity function. For the frequency parameter $F > 10^{-4}$, the branch point is in the lower half of the complex $R$-plane (Points 3, 2 and 1 in Fig. 6). As the Reynolds number increases along the real axis, this branch point is bypassed from the upper side. The second mode (with the phase speed behavior $c \to 1 - 1/M_e$ as $R$ decreases) becomes unstable. Note that both cases correspond to the second-mode instability in terms of Mack's classification.

Figure 7a shows that the receptivity-function maximum, $G_{vib,m} = \max[G_{vib}(R)]$, is close to the lower neutral branch. Figures 7b and 7c illustrate that the function $G_{vib,m}(F)$ has a sharp peak at the frequency $F = 10^{-4}$ corresponding to a singular case when the branch point crosses the real axis (see Point 3 in Fig. 7c). The receptivity functions for suction-blowing perturbations, $G_s$, and temperature perturbations, $G_\theta$, have similar behavior.

Summarizing we conclude that hypersonic boundary-layer on a cooled plate is very sensitive to the vertical velocity perturbations, if they are in resonance with boundary-layer modes. Such perturbations may be induced by suction-blowing through a hole or by skin vibrations. Receptivity to temperature perturbations is relatively low. The receptivity level strongly depends on the forcing locus. The receptivity functions have a sharp peak in the vicinity of the branch point $R_{b1}$. This peak is observed near the lower neutral

branch of the second mode. Singular behavior of the receptivity functions near the point $R_{b1}$ indicates that the foregoing theoretical model should be revised in this case.

**Case 2: Adiabatic wall**

Figures 8a and 8b show the eigenvalue distribution of the second and first modes for the adiabatic plate, $T_w^* = T_{ad}^*$, at the Mach number $M_e = 6.8$. The freestream temperature is $T_e^* = 70.2578$ K, specific heat ratio is $\gamma = 1.4$, Prandtl number is Pr=0.72, second viscosity coefficient is $k = 1.2$, and disturbance frequency parameter is $F = 10^{-4}$. It is seen that the functions $\alpha_r(R)$ and $\alpha_i(R)$ are smoother compared with the cooled wall case shown in Figs. 3a and 3b. This is due to the fact that the spectrum branch points are shifted from the real axis to the complex $R$-plane as shown in Fig. 11.

Figures 9a and 9b show the second-mode increment, $-\alpha_i = -\mathrm{Im}\alpha_2(R)$, and the receptivity functions $G_{vib}(R)$, $G_s(R)$ and $G_\theta(R)$ respectively. Because the first branch point $R_{b1}$ is far from the vibrator center point $R$ (see Point 2 in Fig. 11), receptivity peaks are smoothed out. Nevertheless the receptivity function maximums are still observed near the lower neutral branch.

Figures 10a, 10b, 10c and 10d show distributions of $-\alpha_i(R)$, $G_{vib}(R), G_s(R)$ and $G_\theta(R)$ at various frequency parameters $F$. Imaginary part of the branch point is negative, $\mathrm{Im}(R_{b1}) < 0$, for all frequencies considered (see Fig. 11). As the Reynolds number increases along the real axis, the first branch point is bypassed from the upper side. The second mode (with the phase speed $c \to 1 - 1/M_e$ as $R$ decreases) becomes unstable. Because the second-mode phase speed is less than 1, there is no discontinuity of the receptivity functions as contrasted to the cooled-wall case shown in Figures 5b, 5c and 5d (Curves 4 and 5).

Similar to the cooled plate case, the hypersonic boundary layer is most sensitive to vertical velocity perturbations, if they are in resonance with boundary-layer modes. Receptivity to the surface temperature perturbation is relatively low.

**Estimates of receptivity effectiveness**

To estimate the receptivity effectiveness we consider a two-dimensional vibrator of the shape

$$g(x')=\begin{cases} 0 \text{ at } x'<-l/2, x'>l/2 \\ a \text{ at } -l/2\le x'\le l/2 \end{cases}, \tag{3.11}$$

where $a$ and $l$ is nondimensional amplitude and streamwise length of the vibrator respectively; their dimensional values are expressed as $a^*=a\sqrt{x_0^* \nu_e^* / U_e^*}$ and $l^*=l\sqrt{x_0^* \nu_e^* / U_e^*}$; $x_0^*$ is dimensional coordinate of the vibrator center, which corresponds to $x'=0$. Fourier transform of the shape function (3.11) is expressed in the form

$$\rho(\alpha)=\int_{-\infty}^{+\infty} g(x')\exp(-i\alpha x')dx'=\frac{2a}{\alpha}\sin(\alpha l/2). \tag{3.12}$$

For the resonant wavenumber $\alpha=\alpha_0$, the module $|\rho(\alpha_0)|$ attains its maximum value

$$|\rho(\alpha_0)|=\frac{2a}{\alpha_0} \text{ at } l=\frac{2\pi}{\alpha_0}\left(n+\frac{1}{2}\right),\ n=0,1,2,... \tag{3.13}$$

Then, in accordance with Eq. (3.4), the second-mode wave amplitude is evaluated as

$$Q(x_{10},y_m)=\frac{2a}{\alpha_0}G_{vib}. \tag{3.14}$$

For the adiabatic flat plate, maximum value of the receptivity function is $G_{vib} \approx 5 \cdot 10^{-3}$ at the frequency parameter $F = 10^{-4}$ and Mach number $M_e = 6.8$ (see Fig. 9b); the resonance wavenumber is $\alpha_0 = 0.097 \approx 0.1$ (see Fig. 9a). In this case, *the vibrator of amplitude* $a^* \approx 0.01\sqrt{x_0^* \nu_e^* / U_e^*}$ *induces the second-mode wave of initial amplitude* $Q_{in}(x_0, \alpha_0) \approx 0.1\%$. For a typical hypersonic wind tunnel with the unit Reynolds number $\mathrm{Re}_1 = 10^7$ 1/m, such a vibrator has the amplitude $a^* = 10^{-6}$ m and length $l^* \approx 3$ mm, if it is located near the lower neutral branch point $x^* \approx 0.1$ m.

Note that the highest receptivity occurs near the low neutral branch. Normal waves generated in this region become unstable immediately behind the force element and can achieve critical amplitudes earlier than those generated by other external disturbances far from the neutral branch.

## 4. Receptivity near the spectrum branch point

In Sections 2 and 3, we found that the receptivity function tends to infinity as the resonance point tends to the branch point. This singularity indicates that the receptivity model developed in Section 2 should be revised in the branch point vicinity.

In this Section, we analyze the distributed excitation of the second-mode wave by force waves when the resonance point tends to the branch point. Then we consider the instability excitation produced by a local force element placed near the branch point.

### *4.1 Spectrum behavior*

We briefly discuss the discrete spectrum behavior in the branch-point vicinity. We assume that two modes, say Mode 1 and Mode 2, coincide at the branch point $x_1 = x_{1b}$; *i.e.* $\alpha_1(x_{1b}) = \alpha_2(x_{1b}) = \alpha_b$. As shown in [13] and [21], such branching is typical for

hypersonic boundary layers, when the first mode (Tollmien-Schlichting wave) and the Mack second mode coexist. Near the branch-point, eigenvalues of Modes 1 and 2 are expanded as

$$\alpha_{1,2} = \alpha_b \pm i\lambda\sqrt{x_1 - x_{1b}} + \ldots, \tag{4.1a}$$

Hereafter the subscript $b$ denotes quantities at the first branch point located near the lower neutral branch.

Analysis of numerical examples shown in Figs. 3a, 3.b and 8a, 8b indicates that $|\mathrm{Im}(\lambda)| << |\mathrm{Re}(\lambda)|$; *i.e.* Modes 1 and 2 are almost neutral upstream from the branch point. For simplicity we consider the case when the parameters $\lambda$ and $x_{1b}$ are real and positive. For $x_1 < x_{1b}$, the eigenvalues are determined as

$$\alpha_{1,2} = \alpha_b \mp \lambda\sqrt{x_{1b} - x_1} + \ldots \tag{4.1b}$$

Equation (4.1b) shows that Mode 1 has smaller wavenumber (larger phase speed) than Mode 2 in the upstream region $x_1 < x_{1b}$. If the branch point is bypassed from the upper side, then

$$\alpha_{1,2} = \alpha_b \pm i\lambda\sqrt{x_1 - x_{1b}} + \ldots \text{ for } x_1 > x_{1b} \tag{4.1c}$$

In this case, Mode 1 is stable ($\mathrm{Im}(\alpha_1) > 0$) and Mode 2 is unstable ($\mathrm{Im}(\alpha_2) < 0$) downstream from the branch point.

If the branch point is bypassed from the lower side, then

$$\alpha_{1,2} = \alpha_b \mp i\lambda\sqrt{x_1 - x_{1b}} + \ldots \text{ for } x_1 > x_{1b} \tag{4.1d}$$

In this case, Mode 1 is unstable ($\mathrm{Im}(\alpha_2)<0$) and Mode 2 is stable ($\mathrm{Im}(\alpha_1)>0$) downstream from the branch point. Note that in both cases the unstable mode is Mack's second mode. Without loss of generality we consider the second case assuming that Mode 1 is unstable downstream from the branch point $x_{1b}$ and the eigenvalue behavior is determined by Eqs. (4.1a), (4.1b) and (4.1d).

As the streamwise coordinate $x_1$ tends to the branch point, Mode 1 strongly interacts with Mode 2 due to nonparallel effects. This interaction can be described by the two-mode approximation; *i.e.* the disturbance amplitude from (2.4) is expressed in the form

$$\vec{F}(x_1,y)=c_1(x_1)\vec{A}_1(x_1,y)\exp(\varepsilon^{-1}iS_1)+c_2(x_1)\vec{A}_2(x_1,y)\exp(\varepsilon^{-1}iS_2), \quad (4.2)$$

$$S_{1,2}=\int_{x_{1b}}^{x_1}\alpha_{1,2}(x_1)dx_1 .$$

As shown in Ref. [21], the amplitude coefficients $c_{1,2}(x_1)$ are solutions of the ODE problem

$$\frac{dc_1}{dx_1}=c_1W_{11}+c_2W_{12}\exp[\varepsilon^{-1}i(S_2-S_1)], \quad (4.3a)$$

$$\frac{dc_2}{dx_1}=c_2W_{22}+c_1W_{21}\exp[\varepsilon^{-1}i(S_1-S_2)], \quad (4.3b)$$

$$c_1(x_{1s})=c_{1s},\ c_2(x_{1s})=c_{2s}, \quad (4.3c)$$

where $c_{1s}$ and $c_{2s}$ are prescribed values at a certain initial point $x_{1s}$; the matrix elements are defined as

$$W_{jk}=-\frac{\left\langle \vec{B}_j,\frac{\partial H_0}{\partial\alpha}\frac{\partial\vec{A}_k}{\partial x_1}\right\rangle+i\left\langle \vec{B}_j,H_1\frac{\partial\vec{A}_k}{\partial x_1}\right\rangle}{\left\langle \vec{B}_j,\frac{\partial H_0}{\partial\alpha}\frac{\partial\vec{A}_j}{\partial x_1}\right\rangle},\ j=1,2,\ k=1,2. \quad (4.4)$$

Fedorov and Khokhlov [13], [21] showed that the matrix elements behave as

$$W_{jk} \to \frac{(-1)^{j+k-1}}{4(x_1 - x_{1b})}, \; x_1 \to x_{1b}.$$

That leads to the following singularity of the amplitude coefficients

$$c_{1,2}(x_1) = \frac{C_{1,2}}{(x_1 - x_{1b})^{1/4}} + \ldots \text{ as } x_1 \to x_{1b}, \tag{4.5}$$

where constants $C_{1,2}$ depend on the normalization of eigenfunctions $\vec{A}_{1,2}(x_1, y)$. Note that this singularity is totally determined by the spectrum topology prescribed by Eq. (4.1a). In the first-order approximation, the functions $c_{1,2}(x_1)$ have a universal form in the branch-point vicinity; they do not depend on mean-flow characteristics and disturbance parameters.

In the region, $x_1 - x_{1b} = O(\varepsilon^{2/3})$, the mode decomposition (4.2) is not valid. Introducing the inner variable $\zeta = \varepsilon^{-2/3}(x_1 - x_{1b})$, we can express the local disturbance field in the form

$$\vec{F} = \varepsilon^{-1/6}[c_0(\zeta)\vec{A}_0(y) + \varepsilon^{-1/3}c_{01}(\zeta)\vec{A}_{01}(y) + \ldots]\exp(i\varepsilon^{-1}S_b + i\varepsilon^{-1/3}\alpha_b\zeta), \tag{4.6}$$

where $c_0(\zeta)$ is solution of Airy equation

$$\frac{d^2c_0}{d\zeta^2} - \lambda^2\zeta c_0 = 0. \tag{4.7}$$

Fedorov and Khokhlov [13], [21] matched solutions of Eq. (4.7) with the normal-mode expansions of the outer solution and established an exchange rule for Modes 1 and 2 in the branch-point vicinity.

In the case of real and positive $\lambda$ and $x_{1b}$, a structure of the branch-point influence domain is shown in Fig. 12. It includes three Stokes lines along which the modes are neutral. Within the sector containing the axis portion $x_1 > x_{1b}$, Mode 1 is unstable and Mode 2 is stable, if the branch point is bypassed from the lower side. In accordance with (4.5) and (4.6), the disturbance amplitude has a peak in the influence domain, with maximum amplitude being of the order of $\varepsilon^{-1/6}$. In order to separate this effect from the receptivity mechanism, we need to establish a relationship between the constants $C_{1,2}$ (instead of the amplitude coefficients $c_{1,2}$) and the external force characteristics.

### *4.2 Distributed receptivity*

**Outer solution**

We consider wall perturbations in the traveling-wave form given by Eq. (2.2). If the resonance point $x_{10}$ (where the force wavenumber $\alpha$ coincides with the unstable mode eigenvalue $\alpha_0 = \alpha_1(x_{10})$) is far from the branch point $x_{1b}$, then the normal wave amplitude $\tilde{F}_1$ is given by Eq. (2.25). In the absence of resonance detuning ($\gamma = 0$), this equation is expressed as

$$\tilde{F}_1 = \varepsilon^{-1/2} q \sqrt{\frac{2\pi i}{b}} \vec{A}_1(x_1, y) \exp\left[ i\varepsilon^{-1} \int_{x_{10}}^{x_1} \alpha_1(x_1) dx_1 \right], \quad x_1 > x_{10}, \tag{4.8}$$

where $b$ and $q$ are defined by Eqs. (2.21b) and (2.21c) respectively. Differentiating Eq. (2.10a) with respect to $x_1$ and imposing the solvability condition on the resulting equation we obtain

$$b \equiv \frac{d\alpha_1}{dx_1}(x_{10}) = -\frac{\left\langle \vec{B}_0, \dfrac{\partial H_0}{\partial x_1}(x_{10}, \alpha_0)\vec{A}_0 \right\rangle}{\left\langle \vec{B}_0, \dfrac{\partial H_0}{\partial \alpha}(x_{10}, \alpha_0)\vec{A}_0 \right\rangle}. \tag{4.9}$$

Using this relation we write Eq. (4.8) as

$$\vec{F}_1 = \varepsilon^{-1/2}\sqrt{2\pi i b}\,\frac{(-i)(\vec{\Phi}_0,\vec{B}_0)_{y=0}}{\left\langle \vec{B}_0, \dfrac{\partial H_0}{\partial x_1}(x_{10},\alpha_0)\vec{A}_0 \right\rangle}\,\vec{A}_1(x_1,y)\exp\left[ i\varepsilon^{-1}\int_{x_{10}}^{x_1}\alpha_1(x_1)dx_1 \right],\ x_1 > x_{10}. \tag{4.10}$$

If the resonance point tends to the branch point as $x_{10} \to x_{1b} + 0$, the eigenvalue derivative $b$ is expressed from Eq. (4.1a) in the form

$$b = i\frac{\lambda}{2}(x_{10} - x_{1b})^{-1/2} + \ldots \tag{4.11}$$

Substituting (4.11) into (4.10) we get in the first order approximation

$$\vec{F}_1 = \varepsilon^{-1/2}\,\frac{\sqrt{\pi\lambda}}{(x_{10}-x_{1b})^{1/4}}\,\frac{(\vec{\Phi}_0,\vec{B}_0)_{y=0}}{\left\langle \vec{B}_0, \dfrac{\partial H_0}{\partial x_1}(x_{10},\alpha_0)\vec{A}_0 \right\rangle}\,\vec{A}_1(x_1,y)\exp\left[ i\varepsilon^{-1}\int_{x_{10}}^{x_1}\alpha_1(x_1)dx_1 \right],$$

$$x_1 > x_{10}. \tag{4.12}$$

Comparing (4.12) with (4.2) and (4.5) we express the amplitude coefficient of the unstable Mode 1 in the form

$$C_1 = \varepsilon^{-1/2}\sqrt{\pi\lambda}\,\frac{(\vec{\Phi}_0,\vec{B}_0)_{y=0}}{\left\langle \vec{B}_0, \dfrac{\partial H_0}{\partial x_1}(x_{1b},\alpha_b)\vec{A}_0 \right\rangle}\ \text{as}\ x_{10} \to x_{1b}. \tag{4.13}$$

Equation (4.13) shows that ***distributed receptivity has no singularity at the spectrum branch point.*** In accordance with Eq. (4.5), the disturbance peak is totally due to a singular behavior of the unstable mode itself. If one measures the disturbance amplitude $Q$ at a certain fixed point downstream from the branch point for various locations of the resonant point $x_{10}$, then he will not observe a peak in the distribution

$Q(x_{10})$ at the point $x_{10} = x_{1b}$. However, the function $Q(x_{10})$ will have a maximum at the lower neutral branch because of a different amplification history associated with the exponential term in Eq. (4.2). Since the branch point $x_{1b}$ is close to the lower neutral branch, this maximum will be observed at $x_{10} \approx x_{1b}$.

**Inner solution**

We assume that the forcing wavenumber $\alpha$ satisfies the resonance condition near the branch point; *i.e.* $\alpha = \alpha_b + \varepsilon^{1/3}\gamma$. Here the parameter $\gamma = O(1)$ characterizes resonance detuning. In the branch-point vicinity, the disturbance field is represented in the form

$$\vec{F} = [\varepsilon^{-2/3} c_b(\zeta)\vec{A}_b(y) + \varepsilon^{-1/3} c_{01}(\zeta)\vec{A}_{01}(y) + \ldots + \vec{A}_v(\zeta, y)]\exp(i\varepsilon^{-1/3}\alpha_b\zeta). \quad (4.14)$$

Eigenfunction $\vec{A}_b(y)$ is a solution of the homogeneous problem (2.10). In turn, the function $\vec{A}_{01}(y)$ is a solution of the equation

$$\left(\frac{\partial}{\partial y} - H_0(x_{1b}, \alpha_b)\right)\vec{A}_{01} - \frac{\partial H_0}{\partial \alpha}(x_{1b}, \alpha_b)\vec{A}_b = 0. \quad (4.15)$$

Substituting the expansion (4.14) into Eqs. (2.5)-(2.7) we obtain

$$\left(\frac{\partial}{\partial y} - H_0(x_{1b}, \alpha_b)\right)c_{01}\vec{A}_{01} + i\frac{dc_b}{d\zeta}\frac{\partial H_0}{\partial \alpha}(x_{1b}, \alpha_b)\vec{A}_b = 0. \quad (4.16)$$

From Eqs. (4.15) and (4.16) we derive the relationship

$$c_{01}(\zeta) = -i\frac{dc_b}{d\zeta}. \quad (4.17)$$

Expanding the matrix $H_0$ in the vicinity of $x_{1b}$ we obtain the following problem for the forcing term $\vec{A}_v$

$$\left(\frac{\partial}{\partial y}-H_0(x_{1b},\alpha_b)\right)\vec{A}_v+\frac{d^2c_b}{d\zeta^2}\left[\frac{1}{2}\frac{\partial^2 H_0}{\partial\alpha^2}(x_{1b},\alpha_b)\vec{A}_b+\right.$$

$$\left.\frac{\partial H_0}{\partial\alpha}(x_{1b},\alpha_b)\vec{A}_{01}\right]-c_b\zeta\frac{\partial H_0}{\partial x_1}(x_{1b},\alpha_b)\vec{A}_b=0, \tag{4.18a}$$

$$(A_v)_{1,3,5,7}=\varphi_{1,2,3,4}(x_{1b})\exp(i\gamma\zeta)\text{ at }y=0, \tag{4.18b}$$

$$\left|\vec{A}_v\right|\to 0\text{ at }y\to\infty. \tag{4.18c}$$

Using a standard approach (see for example [28]) we can express the problem (4.18) in the form

$$\left(\frac{\partial}{\partial y}-H_0(x_{1b},\alpha_b)\right)\vec{A}_v+\vec{\Phi}_b\Delta(y)e^{i\gamma\zeta}+\frac{d^2c_b}{d\zeta^2}\left[\frac{1}{2}\frac{\partial^2 H_0}{\partial\alpha^2}(x_{1b},\alpha_b)\vec{A}_b+\right.$$

$$\left.\frac{\partial H_0}{\partial\alpha}(x_{1b},\alpha_b)\vec{A}_{01}\right]-c_b\zeta\frac{\partial H_0}{\partial x_1}(x_{1b},\alpha_b)\vec{A}_b=0, \tag{4.19a}$$

$$(A_v)_{1,3,5,7}=0\text{ at }y=0, \tag{4.19b}$$

$$\left|\vec{A}_v\right|\to 0\text{ at }y\to\infty. \tag{4.19c}$$

Solution of this problem is not trivial, if the inhomogeneous term of Eq. (4.19a) is orthogonal to the eigenfunction $\vec{B}_b(y)$ of the conjugate problem. This solvability condition leads to the following equation for the amplitude coefficient $c_b(\zeta)$

$$\frac{d^2c_b}{d\zeta^2}-\lambda^2\zeta c_b+\tilde{q}e^{i\gamma\zeta}=0, \tag{4.20a}$$

$$\lambda^2=\frac{\left\langle\vec{B}_b,\frac{\partial H_0}{\partial x_1}\vec{A}_b\right\rangle_b}{\frac{1}{2}\left\langle\vec{B}_b,\frac{\partial^2 H_0}{\partial\alpha^2}\vec{A}_b\right\rangle_b+\left\langle\vec{B}_b,\frac{\partial H_0}{\partial\alpha}\vec{A}_{01}\right\rangle_b}, \tag{4.20b}$$

$$\tilde{q}=\frac{(\vec{B}_b,\vec{\Phi}_b)_{y=0}}{\frac{1}{2}\left\langle\vec{B}_b,\frac{\partial^2 H_0}{\partial\alpha^2}\vec{A}_b\right\rangle_b+\left\langle\vec{B}_b,\frac{\partial H_0}{\partial\alpha}\vec{A}_{01}\right\rangle_b}. \tag{4.20c}$$

If normal waves have zero amplitude in the upstream region, *i.e.* $c_b(\zeta)\to 0$ at $\zeta\to-\infty$, then solution of Eq. (4.20a) is expressed as

$$c_b=-\frac{\pi\tilde{q}}{\lambda^{4/3}}\int_{-\infty}^{s}[Ai(s)Bi(s')-Bi(s)Ai(s')]\exp(i\gamma\lambda^{-2/3}s')ds',\ s=\lambda^{2/3}\zeta, \quad (4.21)$$

where $Ai(s)$ and $Bi(s)$ are Airy functions [29]. For the branch-point influence domain structure shown in Fig. 12, we obtain the following asymptotic expressions in the limit $s\to+\infty$

$$Ai(s)\to\frac{1}{\sqrt{\pi}s^{1/4}}\exp\left(-\frac{2}{3}s^{3/2}\right),\ Bi(s)\to\frac{1}{\sqrt{\pi}s^{1/4}}\exp\left(\frac{2}{3}s^{3/2}\right), \quad (4.22a)$$

$$c_b\to\frac{\sqrt{\pi}\tilde{q}}{\lambda^{4/3}s^{1/4}}\exp\left(\frac{2}{3}s^{3/2}\right)I,\ I=\int_{-\infty}^{+\infty}Ai(s)\exp(i\lambda^{-2/3}\gamma s)ds. \quad (4.22b)$$

Using the integral form of Airy function

$$Ai(s)=\frac{1}{2\pi}\int_{-\infty}^{+\infty}\exp(ius+iu^3/3)du, \quad (4.23)$$

we can evaluate (4.22b) as

$$I=\frac{1}{2\pi}\int_{-\infty}^{+\infty}du\exp(iu^3/3)\int_{-\infty}^{+\infty}\exp(ius+i\lambda^{-2/3}\gamma s)ds=\exp(-i\lambda^{-2}\gamma^3/3). \quad (4.24)$$

Summarizing we conclude that in the branch-point vicinity, $x_1-x_{1b}=O(\varepsilon^{2/3})$, the force wave excites the unstable normal wave of the amplitude

$$\vec{F}_1=\varepsilon^{-1/2}\frac{\tilde{q}\sqrt{\pi}}{\lambda^{3/2}(x_1-x_{1b})^{1/4}}\exp\left(-i\frac{\gamma^3}{3\lambda^2}\right)\vec{A}_1(x_1,y)\exp\left[\varepsilon^{-1}\int_{x_{1b}}^{x_1}i\alpha_1(x_1)dx_1\right], \quad (4.25)$$

$$\varepsilon^{2/3}<<x_1-x_{1b}<<1.$$

From Eqs. (4.20b), (4.20c) we get

$$\frac{\tilde{q}}{\lambda^2} = \frac{(\vec{B}_b, \vec{\Phi}_b)_{y=0}}{\left\langle \vec{B}_b, \frac{\partial H_0}{\partial x_1}(x_{1b}, \alpha_b)\vec{A}_b \right\rangle}. \tag{4.26}$$

Substituting (4.26) into (4.25) we obtain the following expression for the amplitude coefficient at $\gamma = 0$

$$C_1 = \varepsilon^{-1/2}\sqrt{\pi\lambda}\,\frac{(\vec{\Phi}_b, \vec{B}_b)_{y=0}}{\left\langle \vec{B}_b, \frac{\partial H_0}{\partial x_1}(x_{1b}, \alpha_b)\vec{A}_b \right\rangle}. \tag{4.27}$$

Comparing (4.13) with (4.27) we conclude that, in the first order approximation, the inner and outer solutions lead to identical expressions for the amplitude coefficient of unstable normal wave.

### *4.3 Local receptivity*

Now we consider a local force element with the shape function determined by Eq. (2.26). We will analyze receptivity as a function of the distance between the forcing element and the branch point $x_{1b}$.

**Outer solution**

If a three-dimensional force element is far from the branch point $x_{1b}$, then the amplitude $\vec{F}_1$ of unstable wave-packet generated by this element is given by Eq. (2.32). Two-dimensional forcing element excites a normal wave of the amplitude (2.33). Using the expression (2.21c) for $q$, the relation (4.9) for the eigenvalue derivative and the eigenvalue expansion (4.1a) we obtain the following approximation for $q$

$$q=\frac{(\vec{\Phi}_0,\vec{B}_0)_{y=0}}{\left\langle \vec{B}_0,\frac{\partial H_0}{\partial x_1}(x_{10},\alpha_0)\vec{A}_0\right\rangle}\frac{\lambda\rho(\alpha_0)}{2(x_{10}-x_{1b})^{1/2}}\ \text{as}\ x_{10}\to x_{1b}. \tag{4.28}$$

Then the amplitude coefficient from Eq. (4.5) is expressed in the branch point vicinity as

$$C_1=\frac{(\vec{\Phi}_0,\vec{B}_0)_{y=0}}{\left\langle \vec{B}_0,\frac{\partial H_0}{\partial x_1}(x_{10},\alpha_0)\vec{A}_0\right\rangle}\frac{\lambda\rho(\alpha_0)}{2(x_{10}-x_{1b})^{1/4}}\ \text{as}\ x_{10}\to x_{1b} \tag{4.29}$$

Local receptivity increases proportionally to $(x_{10}-x_{1b})^{-1/4}$, as the force locus tends to the branch point. This effect is due to the increase of the force wavenumber range involved into the excitation process. In fact, asymptotic expansions are controlled by the parameter $\varepsilon/b$. If the forcing element is far from the branch point, then the eigenvalue derivative $b=O(1)$, and the wavenumber range is estimated as $(\alpha-\alpha_0)=O(\varepsilon^{1/2})$. As the forcing element tends to the branch point, the derivative $b$ tends to infinity in accordance with Eq. (4.11). If the force element is placed in the region $(x_{10}-x_{1b})=O(\varepsilon^{2/3})$, then the wavenumber range becomes of the order of $(\alpha-\alpha_0)=O(\varepsilon^{1/3})$. In this case, Eq. (4.29) indicates that the amplitude coefficient is of the order of $C_1=O(\varepsilon^{-1/6})$.

**Inner solution**

We consider a force element placed in the branch-point influence domain, *i.e.* $(x_{10}-x_{1b})=O(\varepsilon^{2/3})$. According to Eq. (4.25) the normal wave amplitude generated by the forcing wave components $\alpha_b+\varepsilon^{1/3}(\gamma+d\gamma)$ and $\beta+d\beta$ is expressed as

$$d\vec{F}_1=\frac{1}{(2\pi)^2}\varepsilon^{-1/6}\frac{\tilde{q}\sqrt{\pi}}{\lambda^{3/2}(x_1-x_{1b})^{1/4}}\exp\left(-\frac{i\gamma^3}{3\lambda^2}\right)\rho(\alpha_b+\varepsilon^{1/3}\gamma,\beta)\vec{A}_1(x_{1b},y;\beta)\times$$
$$\exp\left(i\alpha_b s+\frac{2}{3}\frac{\lambda(x_1-x_{1b})^{3/2}}{\varepsilon}\right)e^{i\beta z'}d\gamma d\beta. \tag{4.30}$$

Integrating over $\gamma$ and $\beta$ we obtain in the first order approximation

$$\vec{F}_1 = \varepsilon^{-1/6} \int_{-\infty}^{+\infty} \frac{\tilde{q}(x_{1b},\alpha_b)}{4\pi\sqrt{\pi\lambda^3}(x_1 - x_{1b})^{1/4}} J\vec{A}_1(x_1,y;\beta)\exp(i\beta z')\exp\left(i\alpha_b s + \frac{2}{3}\frac{(x_1 - x_{1b})^{3/2}}{\varepsilon}\right)d\beta \tag{4.31}$$

where the integral $J$ is evaluated as

$$J = \int_{-\infty}^{+\infty} \rho(\alpha_b + \varepsilon^{1/3}\gamma,\beta)\exp\left(-i\frac{\gamma^3}{3\lambda^2}\right)d\gamma = \frac{1}{\sqrt{3}}\rho(\alpha_b,\beta)\left(3\lambda^2\right)^{1/3}\Gamma(1/3), \tag{4.32}$$

where Gamma-function is $\Gamma(1/3) = 2.678938\ldots$

In the case of a two-dimensional forcing, the integral (4.31) can be expressed in the compact form

$$\vec{F}_1 = \varepsilon^{-1/6}\frac{\lambda\rho(\alpha_b)\Gamma(1/3)}{2\sqrt{\pi}(x_1 - x_{1b})^{1/4}}\left(\frac{\lambda}{3}\right)^{1/6}\frac{(\vec{B}_b,\vec{\Phi}_b)_{y=0}}{\left\langle \vec{B}_b, \frac{\partial H_0}{\partial x_1}\vec{A}_b\right\rangle_b}\vec{A}_1(x_1,y)\exp\left(i\int_{x_{10}}^{x_1}\alpha_1(x_1)dx_1\right), \tag{4.33}$$

where $\varepsilon^{2/3} << x_1 - x_{1b} << 1$. From this expression and Eq. (4.5) we obtain the following amplitude coefficient

$$C_1 = \left(\frac{\lambda}{3\varepsilon}\right)^{1/6}\frac{\lambda\rho(\alpha_b)\Gamma(1/3)}{2\sqrt{\pi}}\frac{(\vec{B}_b,\vec{\Phi}_b)_{y=0}}{\left\langle \vec{B}_b, \frac{\partial H_0}{\partial x_1}\vec{A}_b\right\rangle_b}. \tag{4.34}$$

***Summarizing we conclude that local receptivity strongly depends on a distance between the forcing element and the branch point. As*** $x_{10} \to x_{1b}$, ***the amplitude coefficient*** $C_1$ ***increases proportionally to*** $|x_{10} - x_{1b}|^{-1/4}$ ***(in accordance with Eq.***

***(4.29)) and attains its maximum value of the order of*** $\varepsilon^{-1/6}$ ***at the point*** $x_{10} = x_{1b}$ ***(in accordance with Eq. (4.34)).*** If one measures the disturbance amplitude $Q$ at a certain fixed point $x_{1*}$ downstream from the branch point for various locations of the forcing element, then he will observe a local peak in the distribution $Q(x_{10})$ at the point $x_{10} = x_{1b}$, which is close to the lower neutral branch. This peak will be enhanced by the maximum of $Q(x_{10})$ due to the amplification history in the region $x_{10} < x_1 < x_{1*}$ associated with the exponential term in Eq. (4.2). Such an experiment may be conducted on a cooled flat plate at the Mach number, wall temperature ratio and disturbance frequency corresponding to the case when the spectrum branch point is close to the real axis. For example, Fig. 4c shows such a regime at $M_e = 5.95$, $T_w / T_{ad} = 0.1$ and frequency parameter $F = 10^{-4}$ (see Point 3).

### 4.4 Results

We consider excitation of Mack's second mode by two-dimensional local forcing. As discussed in Subsection 3.3, this mode may be Mode 1 or Mode 2 depending on the branch-point bypass. For a force element located far from the branch point, the receptivity functions $G_{vib}$, $G_s$, and $G_\theta$ are determined by Eqs. (3.5), (3.7) and (3.9) respectively. If the force element is close to the branch point, $\varepsilon^{2/3} << |x_{10} - x_{1b}| << 1$, then the amplitude coefficient is determined by Eq. (4.29).

In order to separate the receptivity mechanism from the mode singularity at the branch point, we normalize the receptivity function as

$$\overline{G}(x_{10}, x_{1b}, \alpha_b) = G(x_{10}, x_{1b}, \alpha_b) |x_{10} - x_{1b}|^{1/4}. \qquad (4.35)$$

Using Eq. (4.29) we obtain the following expressions for the receptivity functions in the region $\varepsilon^{2/3} << |x_{10} - x_{1b}| << 1$:

for vibrations

$$\overline{G}_{vib}(x_{1b},\alpha_b)=\left|Q_b(y_m)\frac{(U'B_{b,1}+i\omega B_{b,3}+T'B_{b,5})_{y=0}}{\left\langle\frac{\partial H_0}{\partial x_1}(x_{1b},\alpha_b)\vec{A}_b,\vec{B}_b\right\rangle}\frac{\lambda}{2(x_{10}-x_{1b})^{1/4}}\right|, \quad (4.36a)$$

for suction-blowing through a slot

$$\overline{G}_s(x_{1b},\alpha_b)=\left|Q_b(y_m)\frac{(B_{b,3})_{y=0}}{\left\langle\frac{\partial H_0}{\partial x_1}(x_{1b},\alpha_b)\vec{A}_b,\vec{B}_b\right\rangle}\frac{\lambda}{2(x_{10}-x_{1b})^{1/4}}\right|, \quad (4.36b)$$

for surface temperature perturbation

$$\overline{G}_\theta(x_{1b},\alpha_b)=\left|Q_b(y_m)\frac{(B_{b,5})_{y=0}}{\left\langle\frac{\partial H_0}{\partial x_1}(x_{1b},\alpha_b)\vec{A}_b,\vec{B}_b\right\rangle}\frac{\lambda}{2(x_{10}-x_{1b})^{1/4}}\right|. \quad (4.36c)$$

Here subscript "$b$" denotes quantities at the branch point where Mode 1 and Mode 2 have identical eigenvalues and eigenfunctions.

If a force element is placed at the branch point, $x_{1b}=x_{10}$, then we get from Eq. (4.34):

for vibrations

$$\overline{G}_{vib}(x_{1b},\alpha_b)=\left|Q_b(y_m,x_{1b})\frac{(U'B_{b,1}+i\omega B_{b,3}+T'B_{b,5})_{y=0,x_1=x_{1b}}}{\left\langle\frac{\partial H_0}{\partial x_1}(x_{1b},\alpha_b)\vec{A}_b,\vec{B}_b\right\rangle}\frac{\lambda}{2\sqrt{\pi}}\Gamma(1/3)\left(\frac{\lambda}{3\varepsilon}\right)^{1/6}\right|, \quad (4.37a)$$

for suction-blowing

$$\overline{G}_s(x_{1b},\alpha_b)=\left|Q_b(y_m)\frac{(B_{b,3})_{y=0}}{\left\langle\frac{\partial H_0}{\partial x_1}(x_{1b},\alpha_b)\vec{A}_b,\vec{B}_b\right\rangle}\frac{\lambda}{2\sqrt{\pi}}\Gamma(1/3)\left(\frac{\lambda}{3\varepsilon}\right)^{1/6}\right|, \quad (4.37b)$$

for surface temperature perturbation

$$\overline{G}_\theta(x_{1b},\alpha_b)=\left|Q_b(y_m)\frac{(B_{b,5})_{y=0}}{\left\langle\frac{\partial H_0}{\partial x_1}(x_{1b},\alpha_b)\vec{A}_b,\vec{B}_b\right\rangle}\frac{\lambda}{2\sqrt{\pi}}\Gamma(1/3)\left(\frac{\lambda}{3\varepsilon}\right)^{1/6}\right|. \quad (4.37c)$$

We determine the global length scale as $L=\mathrm{Re}(x_b^*)$. Then the branch-point coordinate is $x_{1b}=1$, and $x_1=(R/R_b)^2$. Receptivity functions $\overline{G}_{vib}$, $\overline{G}_s$ and $\overline{G}_\theta$ have been calculated in the branch point vicinity at the following parameters: local Mach number $M_e=5.95$, flow temperature $T_e^*=70.2578$ K, wall temperature ratio $T_w^*/T_e^*=0.69539$, specific heat ratio $c_p/c_v=1.4$, Prandtl number Pr=0.72, and second viscosity coefficient $k=1.2$. These parameters correspond to the case considered in Section 3 and illustrated in Figure 3.

Figures 13a-13e show the receptivity function $\overline{G}_{vib}(x_{10})$ near the branch point $x_{1b}=1$ for the frequency parameter $F\times10^4=0.6$, 0.8, 1.0, 1.2, and 1.4 respectively. Dotted line shows the function $\overline{G}_{vib}(x_{10})$ calculated using the outer solution given by Eq. (3.5); solid line with square symbols shows the asymptotic behavior determined by Eq. (4.36a); open circle shows the quantity $\overline{G}_{vib}(x_{10}=x_{1b})$ given by Eq. (4.37a). Figures 13a and 13b correspond to the case when the branch point is slightly shifted to the lower half of the complex $x_1$-plain (see Points 1, 2 in Fig. 6). Figure 13c illustrates the case when the branch point is very close to the real axis (see Point 3 in Fig. 6). Figures 1d and 1e show the case when the branch point is slightly shifted to the upper half of the complex $x_1$-plain (see Points 4, 5 in Fig. 6).

In all cases under consideration, the imaginary part of the branch point is much smaller than its real part; *i.e.* the real axis crosses the branch-point influence domain $x_1-x_{1b}=O(\varepsilon^{2/3})$ schematically shown in Fig. 12. Because the parameter $\lambda$ is relatively small (its value is about $2.5\times10^{-2}$), the asymptotic parameter $(\lambda/\varepsilon)^{1/6}$, which actually controls the receptivity maximum given by Eq. (4.37a), is not very large. It is $(\lambda/\varepsilon)^{1/6}\approx4.3$ at the frequency parameter $F=6\times10^{-5}$ and $(\lambda/\varepsilon)^{1/6}\approx3.2$

at $F = 1.4 \times 10^{-4}$. This explains relatively low value of $\overline{G}_{vib}(x_{10} = x_{1b})$, which restricts receptivity peaks at the branch point. Similar reasoning helps to explain the difference between asymptotic curves (solid lines with square symbols) and actual behavior of the outer solution (dotted lines). Nevertheless our asymptotic model captures basic features of the branch-point effect and allows us to estimate receptivity peaks in the branch-point vicinity.

Figure 14 shows the receptivity maximum $\overline{G}(x_{10} = x_{1b})$ versus the frequency parameter for suction-blowing through a two-dimensional slot, $\overline{G} = \overline{G}_s(x_{10} = x_{1b})$; for vibrations, $\overline{G} = \overline{G}_{vib}(x_{10} = x_{1b})$; and surface temperature perturbations, $\overline{G} = \overline{G}_\theta(x_{10} = x_{1b})$. Similar to the case of regular receptivity shown in Fig. 9b (where the force element is far from the branch point), suction-blowing is the most effective source of instability excitation in the branch-point vicinity. Receptivity to temperature perturbations is essentially lower than that to vibrations and suction-blowing. Similar conclusions can be made using distributions of the receptivity maximum with respect to the branch-point locus $\mathrm{Re}(R_b)$ shown in Fig. 15.

## 5. Estimates of critical vibrations for bypass

Sufficiently strong forcing is able to generate such a high level of local disturbances in the excitation region that nonlinear mechanisms can cause early breakdown to turbulence. In this case, the linear stability phase is bypassed and the transition onset occurs just behind the forcing element. To estimate the force level providing bypass we assume that the excitation mechanism is linear up to the critical amplitude $Q_{cr}$ of normal waves.

### *5.1 Local vibrations*

We consider a two-dimensional vibrator of the shape given by Eq. (3.11). Its Fourier transform is determined from Eq. (3.12). For the resonant wavenumber $\alpha = \alpha_0$, the module of Fourier component $\rho(\alpha_0)$ is given by Eq. (3.13).

If the vibrator is far from the branch point, then we can use the results of Section 3. In accordance with Eq. (3.14), the vibrator amplitude providing critical level of mass-flux disturbance $Q_{cr}$ in the excitation region $(x_1 - x_{10}) = O(\varepsilon^{1/2})$ is estimated as

$$a_{cr}(x_{10}) \approx \frac{\alpha_0 Q_{cr}}{2G_{vib}}, \tag{5.1}$$

where $G_{vib}$ is determined by Eq. (3.5).

If the vibrator is placed at the branch point, then we can use the results of Section 4. The critical vibrator amplitude in the excitation region $(x_1 - x_{1b}) = O(\varepsilon^{2/3})$ is estimated as

$$a_{cr}(x_{1b}) \approx \left(\frac{\lambda}{\varepsilon}\right)^{1/6} \frac{\alpha_b Q_{cr}}{2\overline{G}_{vib}}, \tag{5.2}$$

where $\overline{G}_{vib}$ is given by Eq. (4.37a).

For definiteness, we assume that bypass occurs at $Q \geq Q_{cr} = 1\%$. Using this criterion we calculated the critical amplitude $a_{cr}$ as a function of the vibration locus $x_{10}$ expressed in terms of the Reynolds number $R = \sqrt{x_{10}^* U_e^* / \nu_e^*}$.

Figure 16 shows the distribution $a_{cr}(R)$ for adiabatic flat plate at Mach number $M_e = 6.8$; mean-flow parameters correspond to the case shown in Figures 10a and 10b; nondimensional frequency parameter is $F \times 10^4 = 0.6$, 0.8 and 1.4. Since the branch point is relatively far from the real axis, calculations were conducted using Eq. (5.1). Minimum of the function $a_{cr}(R)$ corresponds to the region of maximum receptivity (see Fig. 10b). It is close to the lower neutral branch. Minimum value of $a_{cr}(R)$ is slowly decreases as the vibrator frequency decreases. For the unit Reynolds number $\mathrm{Re}_1 = U_e^* / \nu_e^* = 10^6$ 1/ft and frequency parameter $F = 0.8 \times 10^{-4}$, the dimensional critical amplitude is estimated as $a_{cr}^* = a_{cr}\sqrt{\nu_e^* x^* / U_e^*} \approx 0.001$ inch.

Figure 17 shows the distribution $a_{cr}(R_b)$ for cooled flat plate at Mach number $M_e = 5.95$; mean-flow parameters correspond to the case shown in Figures 14 and 15. Because the branch point is close to the real axis, calculations were conducted using Eq. (5.2). Due to high receptivity in the branch-point vicinity the nondimensional critical amplitude is essentially lower than in the previous case. For the unit Reynolds number $\mathrm{Re}_1 = U_e^* / \nu_e^* = 10^6$ 1/ft and frequency parameter $F = 0.8 \times 10^{-4}$, the dimensional critical amplitude is estimated as $a_{cr}^* \approx 0.0007$ inch.

These examples show that local vibrations of the resonance frequency are effective sources of boundary layer tripping. If vibrations are equally available allover the plate surface, initial amplitudes of unstable normal waves are maximal near the lower neutral branch.

### *5.2 Distributed vibrations*

If the vibration spectrum contains discrete components, then the receptivity level may be essentially higher and the critical amplitude may be much smaller than in the case of local vibrations. This situation may occur when one of discrete modes of skin structure vibrations is in resonance with the boundary-layer modes.

If the resonance point is far from the branch point, then the critical amplitude of the vibrational mode is evaluated from Eq. (2.25) as

$$a_{cr} \approx \frac{Q_{cr}}{G_{vib}} \left( \frac{\varepsilon b}{2\pi} \right)^{1/2}, \tag{5.3}$$

where $b$ and $G_{vib}$ are given by Eqs. (2.21b) and (3.5) respectively. Using Eq. (4.9) we can express the critical amplitude in the explicit form

$$a_{cr} \approx \frac{Q_{cr}}{E_{vib}} \left( \frac{\varepsilon}{2\pi b} \right)^{1/2}, \tag{5.4}$$

$$E_{vib}(x_{10},\alpha_0)=\left|Q_2(y_m,x_{10})\frac{(U'B_{2,1}+i\omega B_{2,3}+T'B_{2,5})_{y=0,x_1=x_{10}}}{\left\langle\frac{\partial H_0}{\partial x_1}(x_{10},\alpha_0)\vec{A}_2,\vec{B}_2\right\rangle}\right|.$$

If the resonance point coincides with the branch point, then the mass-flux disturbance amplitude is estimated from Eqs. (4.14) and (4.21) as

$$Q\approx\varepsilon^{-2/3}a\frac{\pi\tilde{q}}{\lambda^{4/3}}Q_2(y_m,x_{1b}). \tag{5.5}$$

Using Eq. (4.26) we obtain

$$Q\approx\left(\frac{\varepsilon}{\lambda}\right)^{-2/3}aE_{vib}(x_{1b}), \tag{5.6}$$

$$E_{vib}(x_{1b})=\pi\left|Q_2(y_m,x_{1b})\frac{(U'B_{b,1}+i\omega B_{b,3}+T'B_{b,5})_{y=0,x_1=x_{1b}}}{\left\langle\vec{B}_b,\frac{\partial H_0}{\partial x_1}\vec{A}_b\right\rangle_b}\right|.$$

Then the critical amplitude of the vibrational mode is estimated as

$$a_{cr}\approx\left(\frac{\varepsilon}{\lambda}\right)^{2/3}\frac{Q_{cr}}{E_{vib}(x_{1b})}. \tag{5.7}$$

Figure 18 shows the distribution $a_{cr}(R)$ evaluated from Eq. (5.4) for adiabatic flat plate at Mach number $M_e=6.8$; mean-flow parameters correspond to the case shown in Figures 10a and 10b; the frequency parameter is $F\times10^4=0.6$, 0.8 and 1.4. Comparing these data with the distributions shown in Fig. 16 we conclude that the critical amplitude of the vibrational discrete mode is much less than that of the local vibrator. For the unit Reynolds number $\mathrm{Re}_1=U_e^*/\nu_e^*=10^6$ 1/ft and frequency

parameter $F = 0.8 \times 10^{-4}$, the dimensional critical amplitude is estimated as $a_{cr}^* = a_{cr}\sqrt{\nu_e^* x^* / U_e^*} \approx 6.6 \times 10^{-5}$ inch.

Figure 19 shows the distribution $a_{cr}(R_b)$ for cooled flat plate at Mach number $M_e = 5.95$; mean-flow parameters correspond to the case shown in Figures 14 and 15. Because the branch point is close to the real axis, calculations were conducted using Eq. (5.7). Nondimensional critical amplitudes are essentially lower than in the previous case. For the unit Reynolds number $\mathrm{Re}_1 = U_e^* / \nu_e^* = 10^6$ 1/ft and frequency parameter $F = 0.8 \times 10^{-4}$, the dimensional critical amplitude is $a_{cr}^* \approx 9.3 \times 10^{-6}$ inch. These examples indicate that discrete vibrational modes of the resonance frequency and wavelength are extremely effective sources for the boundary layer tripping.

## 6. Summary discussion

This study addresses theoretical modeling of hypersonic boundary layer receptivity to wall-induced perturbations on a flat plate. Since the receptivity problem depends on different scales and includes small parameters, we used a combination of asymptotic and numerical methods. Asymptotic analysis allows us to obtain compact analytical relations for the receptivity function, identify governing nondimensional parameters and establish basic features of the receptivity mechanism. Analytical results were integrated in a computationally non-intensive module, which was combined with a standard stability code. This module provides initial amplitudes of normal waves excited by wall disturbances of various types and shapes.

If the discrete spectrum of the boundary-layer disturbances is simple, *i.e.* eigenvalues of normal waves are different, then receptivity to wall forcing of a traveling wave form shows the following features:

- Resonant excitation occurs in narrow regions of the length $l = R_L^{1/2}\delta$.
- Normal-wave amplitude is proportional to $(L/\delta)^{1/2} = R_L^{1/2}$.

- As the Reynolds number increases, nonparallel effects (which disturb the resonance condition) decrease and the relative length of the resonance region, $l/\delta$, increases. In the parallel-flow limit, $R_L \to \infty$, the normal wave amplitude tends to infinity. In this case, the upper limit of disturbance amplitude is determined by nonlinear effects.

These conclusions are consistent with the results of [23] obtained for subsonic boundary layers.

As contrasted to the case of distributed forcing, local forcing generates the boundary-layer disturbance of a finite amplitude even in the parallel flow limit. This is due to the fact that only a small portion of the forcing spectrum, $(\alpha - \alpha_0) = O(\varepsilon^{1/2})$, is involved into the resonance mechanism. As $\varepsilon \to 0$, the resonant excitation increases proportionally to $\varepsilon^{-1/2}$, whereas the spectrum region is narrowed down proportionally to $\varepsilon^{1/2}$. Because both trends compensate each other, the normal-wave amplitude tends to a finite value as $\varepsilon \to 0$. This conclusion is consistent with the results of [25] obtained for subsonic boundary layers.

Calculations showed that a hypersonic boundary layer is very sensitive to vertical velocity perturbations to be in resonance with the boundary-layer normal waves. Such perturbations may be induced by suction-bowing through a hole or slot as well as by skin vibrations. Receptivity to surface temperature perturbations is relatively low. For adiabatic flat plate at Mach number $M_e = 6.8$, a two-dimensional vibrator of the length $l \approx \pi/\alpha_0$, amplitude $a^* \approx 0.01\sqrt{x_0^* \nu_e^* / U_e^*}$ and frequency $F = 10^{-4}$ induces the second-mode wave of the initial mass-flux amplitude $Q_{in}(x_0, \alpha_0) \approx 0.1\%$ If nonlinear breakdown begins at the critical amplitude $Q_{cr} \approx 1\%$, then the amplification factor is estimated as $N = \ln(Q_{cr} / Q_{in}) \approx 2.3$. This value is essentially less than the empirical value $N \approx 10$ for "quiet" conditions.

As shown in [13] and [21], discrete spectrum of hypersonic boundary layer has branch points, where eigenvalues of the first and second modes coincide. In the branch-point influence domain, the normal wave decomposition is not valid and should be replaced

by a local solution. In the cooled wall case, the first branch point is located very close the lower neutral branch of the second mode. Both propagation and excitation of normal waves are singular in the branch-point influence domain. The receptivity function tends to infinity as the resonance point approaches the branch point. Asymptotic analysis of this singularity leads to the following conclusions:

- Distributed receptivity to traveling force wave is not singular at the branch point. The receptivity function peak is totally due to a singular behavior of normal waves. If one measures the disturbance amplitude $Q$ at a fixed point downstream from the branch point $x_{1b}$ for various loci of the resonance point $x_{10}$, then he will not observe a peak of the distribution $Q(x_{10})$ at the point $x_{10} = x_{1b}$.

- Local receptivity strongly depends on a distance between the forcing element locus $x_{10}$ and the branch point. As $x_{10} \to x_{1b}$, the normal-wave amplitude increases proportionally to $|x_{10} - x_{1b}|^{-1/4}$ and attains its maximum value of the order of $\varepsilon^{-1/6}$ at $x_{10} = x_{1b}$. If one measures the disturbance amplitude $Q$ at a fixed point downstream from the branch point for various loci of the forcing element, then he will observe a local peak in the distribution $Q(x_{10})$ at the point $x_{10} = x_{1b}$.

Suction-blowing and skin vibrations are very effective sources of the second mode excitation in the branch-point vicinity. Receptivity to surface temperature perturbations is essentially lower.

Critical amplitudes $a_{cr}$ of skin vibrations were estimated for bypass of the linear stability phase. Assuming that bypass occurs at the disturbance level $Q_{cr} = 1\%$, we found that

- for a local two-dimensional vibrator on adiabatic wall at Mach $M_e = 6.8$, the critical amplitude is $a_{cr}^* \approx 0.09\sqrt{\nu_e^* x^* / U_e^*}$ near the lower neutral branch;

- for a local two-dimensional vibrator on cooled wall at Mach $M_e = 5.95$, the critical amplitude is $a_{cr}^* \approx 0.025\sqrt{\nu_e^* x^* / U_e^*}$ near the first branch point;

- for two-dimensional vibrational wave on adiabatic wall at Mach $M_e = 6.8$, critical amplitude is $a_{cr}^* \approx 0.005\sqrt{\nu_e^* x^* / U_e^*}$ near the lower neutral branch;

- for two-dimensional vibrational wave on cooled wall at Mach $M_e = 5.95$, critical amplitude is $a_{cr}^* \approx 0.0004\sqrt{\nu_e^* x^* / U_e^*}$ near the first branch point.

In all cases considered, receptivity maximum corresponds to the lower neutral branch. Normal waves generated in this region start to grow just behind the force element and can achieve critical amplitudes earlier than those generated elsewhere. If wall forcing is equally available allover the plate, receptivity near the lower neutral branch is dominant.

Foregoing examples show that hypersonic boundary layer is extremely sensitive to skin vibrations. This factor should be accounted for transition prediction in active (ascending) flight, when propulsion system may induce skin vibrations of sufficiently high levels. This conclusion is consistent with the transition data [22] obtained on a sharp cone installed on the rocket nose. Transition loci measured during ascending flight are close to those obtained in conventional (noisy) wind tunnels.

Our theoretical model needs to be verified by experiment. This can be done in a hypersonic wind tunnel on a flat plate or sharp cone. An artificial source of local vibrations can be developed using high-frequency piezoceramic elements. Another option is to induce periodic suction-blowing perturbations through a hole using the spark-discharge method developed in the Institute of Theoretical and Applied Mechanics of Novosibirsk [30]. Our theoretical model can help to predict optimal parameters of such elements and estimate disturbance levels to be measured.

Of special interest are the cooled plate regimes, when the branch point effects are most pronounced. These effects can be captured by hot-wire measurements of disturbance field generated by the wall forcing element of a fixed frequency.

Analytical results have been obtained for three-dimensional disturbances. However, the numerical examples addressed two-dimensional cases only. In the majority of

practical cases, disturbance sources are three-dimensional. Calculations of excitation and evolution of unstable wave packets including the branch-point effects may give a new insight into the initial phases of hypersonic boundary-layer transition. Parametrical studies in a wide range of Mach number, pressure gradient, wall temperature ratio and other parameters are also needed.

## References


1. Reshotko, E., "Boundary Layer Instability, Transition and Control," AIAA Paper No. 94-0001, 1994.
2. Morkovin, M.V., "Critical Evaluation of Transition from Laminar to turbulent Shear Layers with Emphasis on Hypersonically Traveling Bodies," AFFDL-TR-68-149, Air Force Flight Dynamics Laboratory, Wright-Patterson AFB, OH, 1969.
3. Hefner, J.N., and Bushnell, D.M., "Application of Stability Theory to Laminar Flow Control," AIAA Paper No. 79-265, 1979.
4. Malik, M., Zang, T., and Bushnell, D, "Boundary Layer Transition in Hypersonic Flows," AIAA Paper No. 90-5232, 1990.
5. Malik, M.R., "COSAL - A Black Box Compressible Stability Analysis Code for Transition Prediction in Three-Dimensional Boundary Layers," NASA CR-165925, May 1982.
6. Bertolotti, F.P., and Herbert, Th., "Analysis of the Linear Stability of Compressible Boundary Layers Using the PSE," *Theoretical and Computational Fluid Dynamics*, Vol. 3, pp. 117-124, 1991.
7. Chang, C.-L., Malik, M.R., Erlebacher, G., and Hussaini, M.Y., "Compressible Stability of Growing Boundary Layers Using Parabolized Stability Equations," AIAA Paper No. 91-1636, 1991.
8. Malik, M.R., and Li, F., "Transition Studies for Swept Wing Flows Using PSE," AIAA Paper No. 93-0077, 1993.
9. Stetson, K.F., and Kimmel, R.L., "The Hypersonic Boundary-Layer Stability," AIAA Paper, No. 92-0737, January, 1992.
10. Kendall, J. M., "Wind Tunnel Experiments Relating to Supersonic and Hypersonic Boundary Layer Transition," *AIAA Journal*, Vol. 13, No. 3, pp. 290-299, 1975.
11. Maslov, A.A., Shiplyuk, A.A., Sidorenko, A.A., and Arnal, D., "Leading Edge Receptivity of the Hypersonic Boundary Layer," Preprint No. 1-97, Inst. of Theoretical and Applied Mechanics, Russian Academy of Sciences Siberian Branch, and Center d'Etudes et de Recherches de Toulouse, Novosibirsk, 1998.

12. Mack, L. M., "Linear Stability Theory and the Problem of Supersonic Boundary-Layer Transition," *AIAA Journal*, Vol. 13, No. 3, pp. 278-289, 1975.
13. Fedorov, A.V., and Khokhlov, A.P., "Excitation and Evolution of Unstable Disturbances in Supersonic Boundary Layer," *Proc. of 1993 ASME Fluid Engineering Conference*, Washington, DC, June 20-24, 1993, FED-Vol. 151, Transitional and Turbulent Compressible Flows, ASME 1993, pp.1-13, 1993.
14. Goldstein, M.E., "The Evolution of Tollmien-Schlichting Waves near a Leading Edge," *J. Fluid Mech.*, Vol. 127, pp. 59-81, 1983.
15. Kendall, J.M., "Boundary Layer Receptivity to Freestream Turbulence," AIAA Paper No. 90-1504, 1990.
16. Choudhari, M., and Streett, C., "Boundary Layer Receptivity Phenomena in Three-Dimensional and High-Speed Boundary Layers," AIAA Paper No. 90-5258, 1990.
17. Saric, W.S., and Reed, H.L., "Leading Edge Receptivity to Sound: Experiments, DNS, and Theory," AIAA Paper No. 94-2222, 1994.
18. Choudhari, M., "Boundary-Layer Receptivity to Three-Dimensional Unsteady Vortical Disturbances in Free Stream," AIAA Paper No. 96-0181, 1996.
19. Choudhari, M., "Theoretical Prediction of Boundary-Layer Receptivity," AIAA Paper No. 94-2223, 1994.
20. Zhong, X., "Direct Numerical Simulation of Hypersonic Boundary Layer Transition over Blunt Leading Edges, Part I: A New Numerical Method and Validation," AIAA Paper No. 97-0755, 1997.
21. Fedorov, A.V., "Laminar Turbulent Transition in a Hypersonic Boundary Layer," EOARD Report SPC-96-4024, July 1997.
22. Skuratov, A.S., Fedorov, A.V., and Shogin, Yu.N., "Analysis of Flight and Wind Tunnel Experimental Data on the Laminar-Turbulent Transition of the Boundary Layer on Sharp Nosed Cones with Smooth and Rough Surface," In Methods of Investigation of Characteristics of Hypersonic Vehicles. Annual TsAGI's Workshop-School "Fluid Dynamics", February 25-March 1, 1992, pp. 171-172.
23. Tumin, A.M., and Fedorov, A.V., "Excitation of Instability Waves by Local Vibrator in Boundary Layer," *J. Prikl. Matem. and Tekh. Fiz.*, No. 6, pp. 65-71, 1984.

24. Gilev, V.M., and Kozlov, V.V., "Excitation of Tollmien-Schlichting Waves by Vibrator in Boundary Layer," Preprint No. 19-83, ITAM SO AN SSSR, Novosibirsk, 1983.

25. Fedorov, A.V., "Excitation of Tollmien-Schlichting Waves in Boundary Layer by Periodic External Forcing Localized on Body Surface," *Izv. AN SSSR, Mekh. Zhidk. i Gaza*, No. 6, pp. 36-41, 1984.

26. Zhigulev, V.N., and Tumin, A.M., *Onset of Turbulence*, Nauka, Novosibirsk, 1987.

27. Nayfeh, A.H., "Stability of Three-Dimensional Boundary Layer," *AIAA Journal*, Vol. 18, No. 4, pp. 406-416, 1980.

28. Vladimirov, V.S., *Equations of Mathematical Physics*, Nauka, Moscow, 1976.

29. Abramovitz, M., and Stegun, I.A., *Handbook of Mathematical Functions*, National Bureau of Standards, Applied Mathematics Series 55, June 1964.

30. Kosinov, A.D., Maslov, A.A., and Shevelkov, S.G., "Experiments on the Stability of Supersonic Laminar Boundary Layers," *J. Fluid Mech.*, Vol. 219, pp. 621-633, 1990.

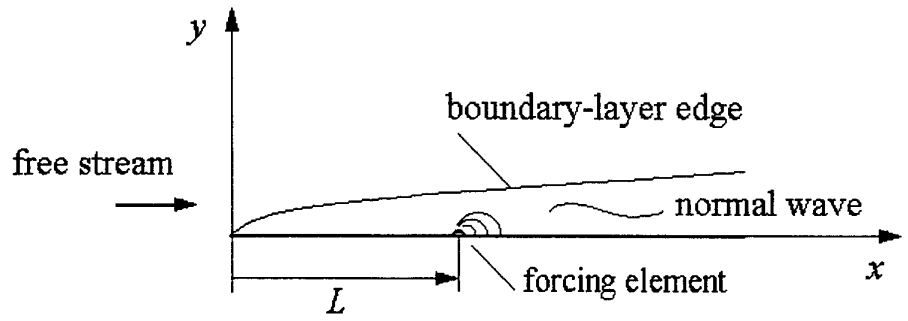


Fig. 1 Flow scheme.

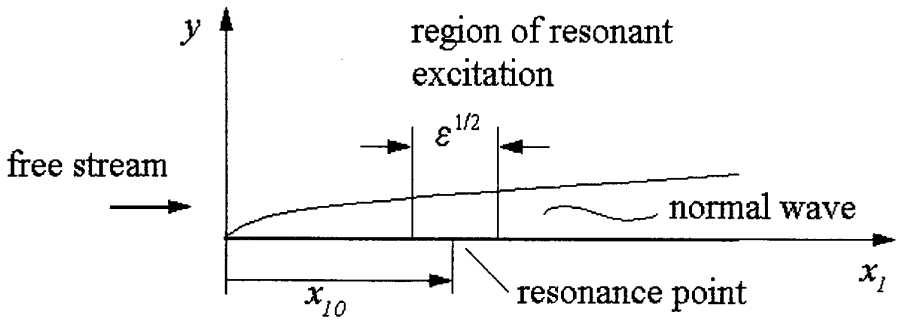


Fig. 2 Flow scheme of resonant excitation.

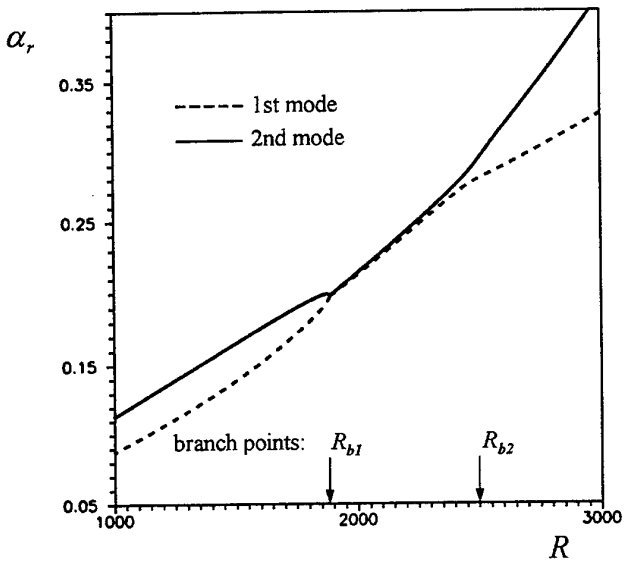


Fig. 3a Disturbance spectrum: $M_e = 5.95$, $T_w / T_{ad} = 0.1$, $F = 10^{-4}$; distributions $\alpha_r(R)$.

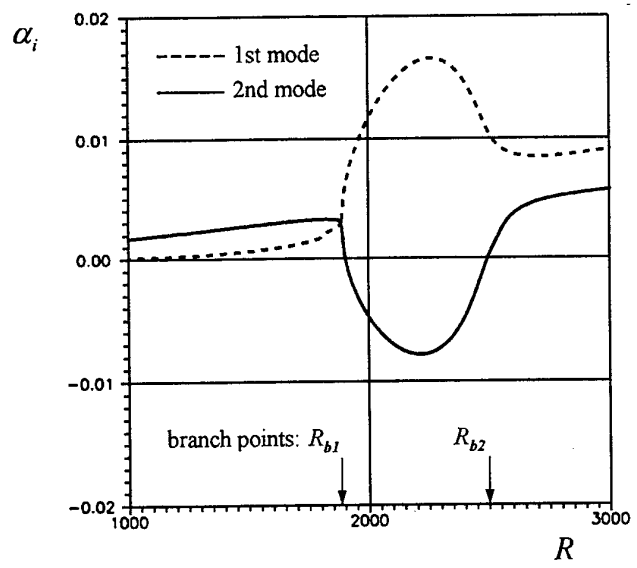


Fig. 3b Disturbance spectrum: $M_e = 5.95$, $T_w / T_{ad} = 0.1$, $F = 10^{-4}$; distributions $\alpha_i(R)$.

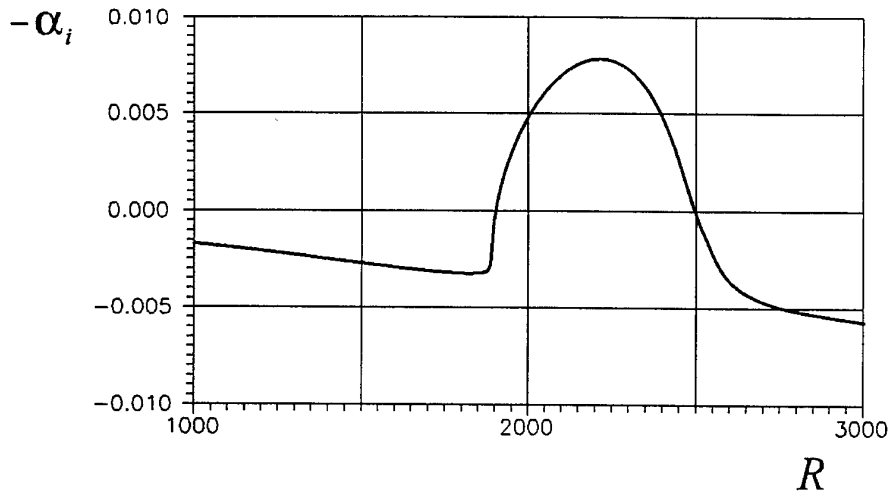


Fig. 4a Second mode increment as a function of Reynolds number: $M_e = 5.95$, $T_w / T_{ad} = 0.1$, $F = 10^{-4}$.

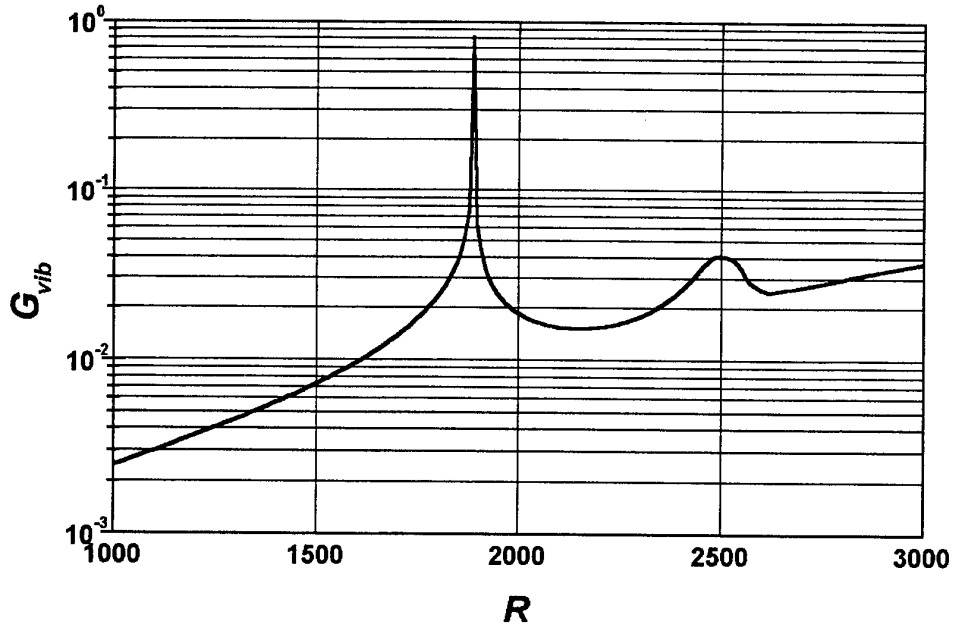


Fig. 4b Receptivity function $G_{vib}(R)$ at $M_e = 5.95$, $T_w / T_{ad} = 0.1$, $F = 10^{-4}$.

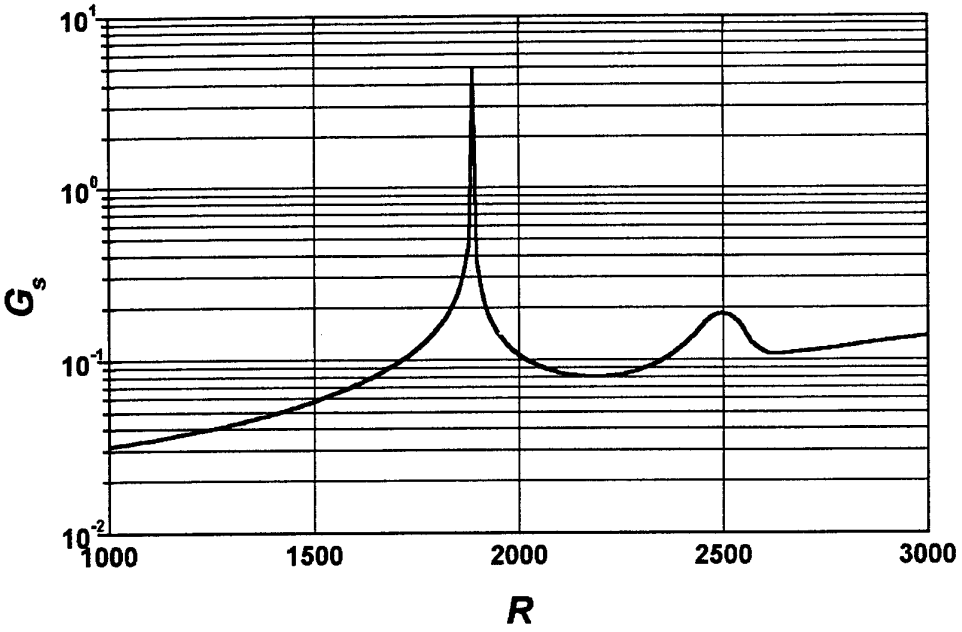


Fig. 4c Receptivity function $G_s(R)$ at $M_e = 5.95$, $T_w / T_{ad} = 0.1$, $F = 10^{-4}$.

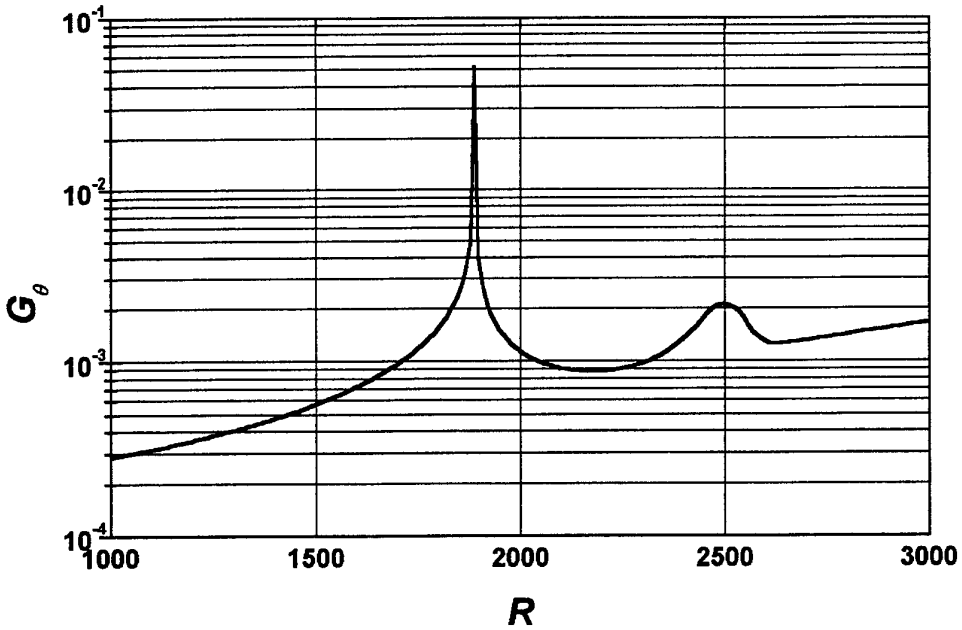


Fig. 4d Receptivity function $G_\theta(R)$ at $M_e = 5.95$, $T_w / T_{ad} = 0.1$, $F = 10^{-4}$.

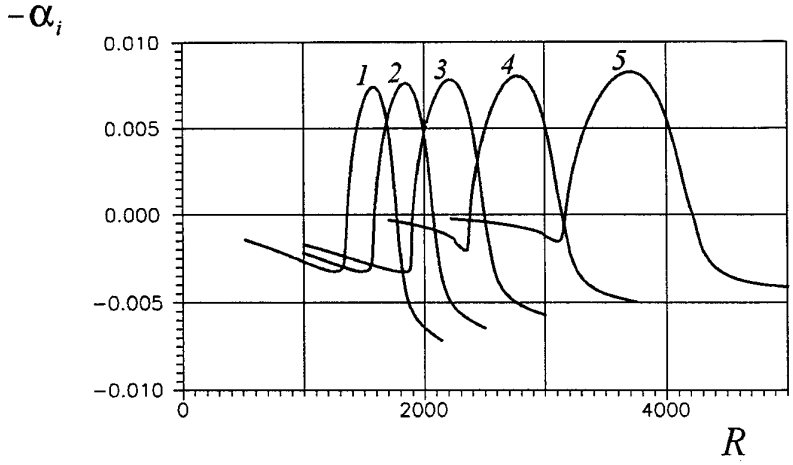


Fig. 5a Second-mode increment as a function of Reynolds number: $M_e = 5.95$, $T_w / T_{ad} = 0.1$; curves 1, 2, 3, 4 and 5 correspond to the frequency parameter $F \times 10^4$ = 1.4, 1.2, 1.0, 0.8 and 0.6 respectively.

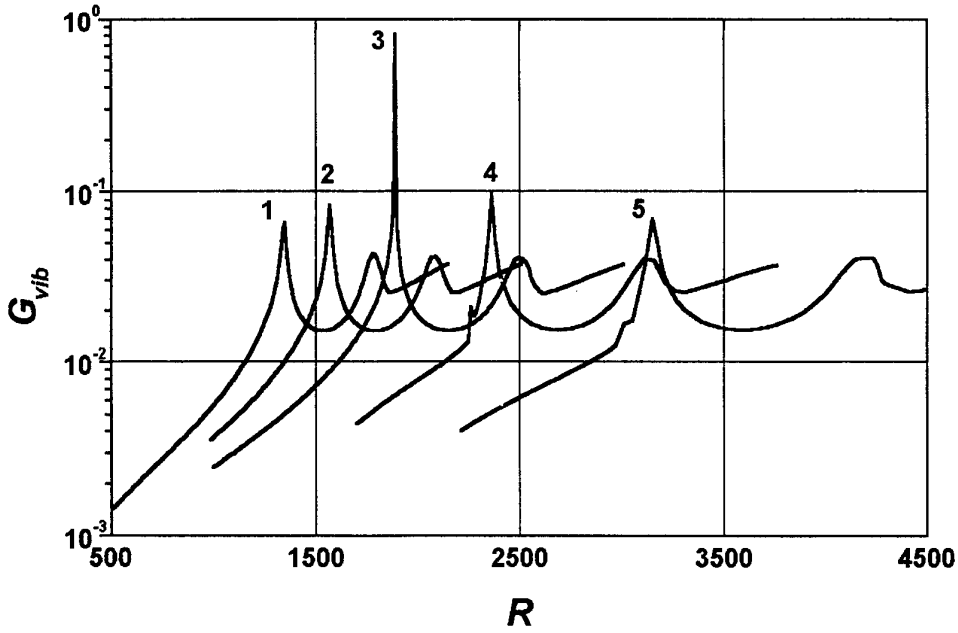


Fig. 5b Receptivity function $G_{vib}(R)$ at $M_e = 5.95$, $T_w / T_{ad} = 0.1$; curves 1, 2, 3, 4 and 5 correspond to $F \times 10^4 = 1.4$, 1.2, 1.0, 0.8 and 0.6 respectively.

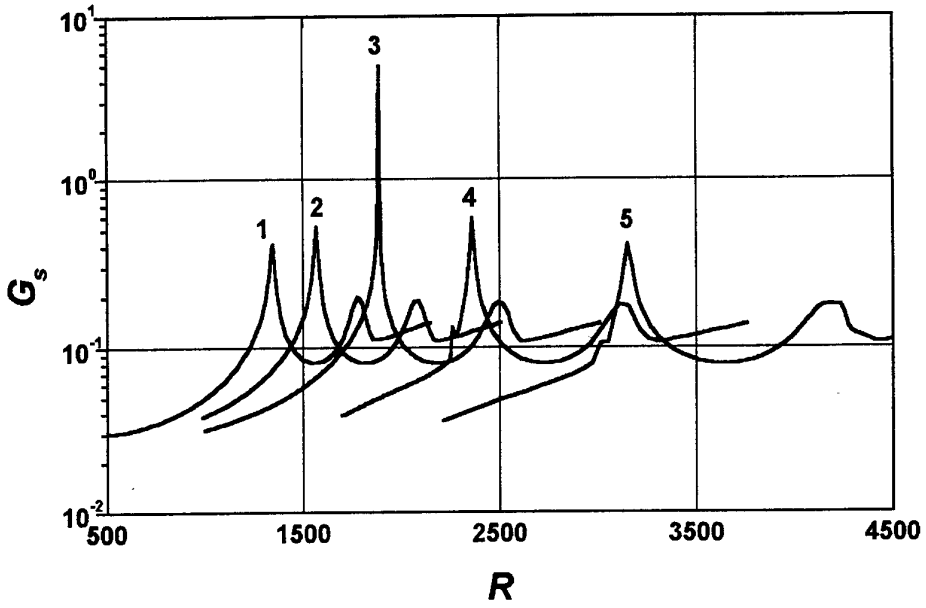


Fig. 5c Receptivity function $G_s(R)$ at $M_e = 5.95$, $T_w / T_{ad} = 0.1$; curves 1, 2, 3, 4 and 5 correspond to $F \times 10^4 = 1.4$, 1.2, 1.0, 0.8 and 0.6 respectively.

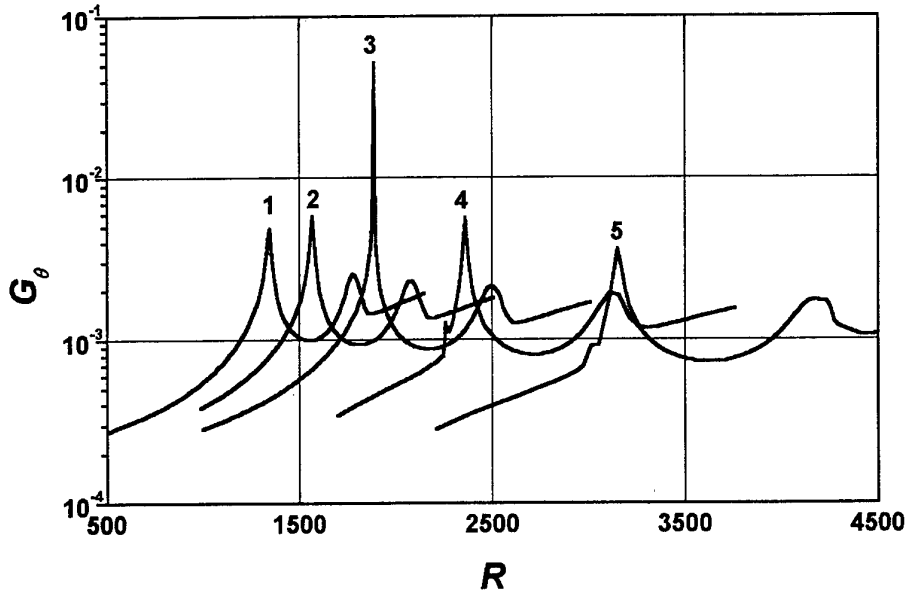


Fig. 5d Receptivity function $G_\theta(R)$ at $M_e = 5.95$, $T_w / T_{ad} = 0.1$; curves 1, 2, 3, 4 and 5 correspond to $F \times 10^4 = 1.4$, 1.2, 1.0, 0.8 and 0.6 respectively.

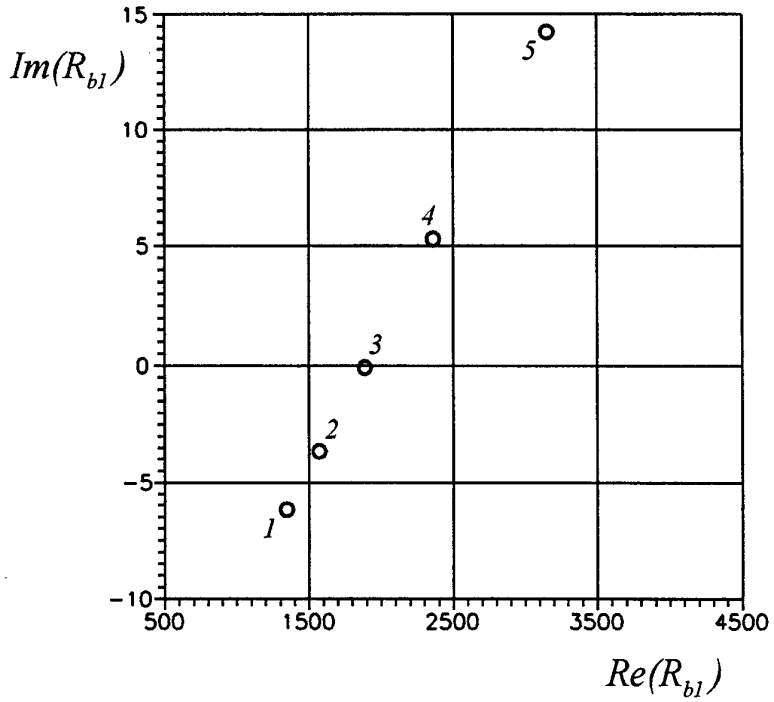


Fig. 6 First branch point locus at $M_e = 5.95$, $T_w / T_{ad} = 0.1$; points 1, 2, 3, 4 and 5 correspond to $F \times 10^4 = 1.4$, 1.2, 1.0, 0.8 and 0.6 respectively.

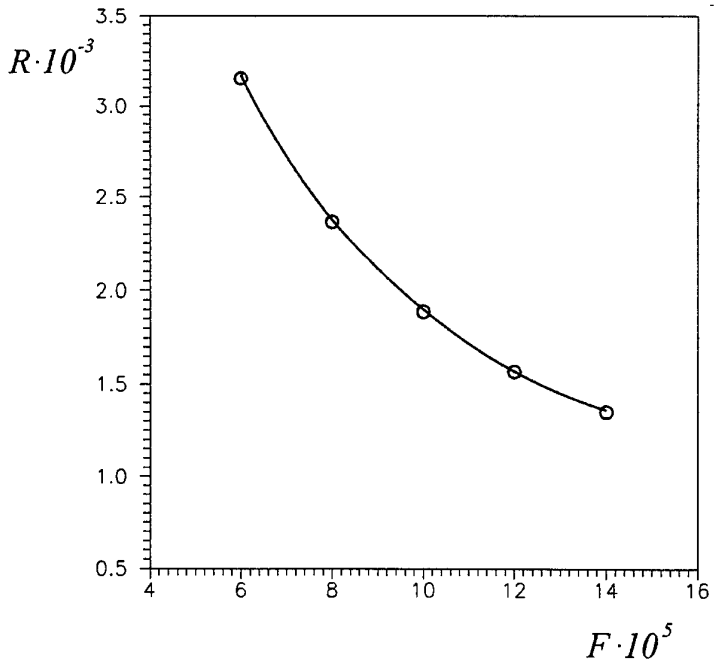


Fig. 7a Locus of the receptivity function maximum (solid line) and the lower neutral branch (symbols): $M_e = 5.95$, $T_w / T_{ad} = 0.1$.

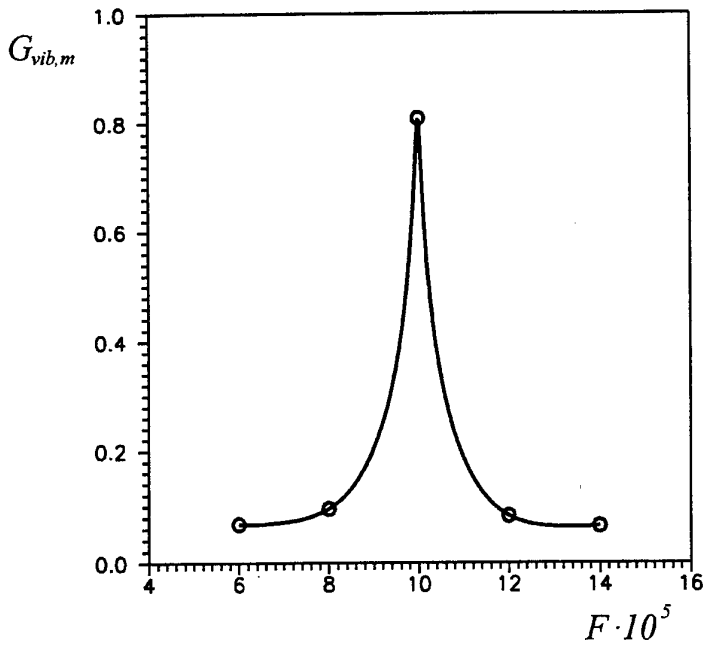


Fig. 7b Receptivity function maximum versus the disturbance frequency: $M_e = 5.95$, $T_w / T_{ad} = 0.1$.

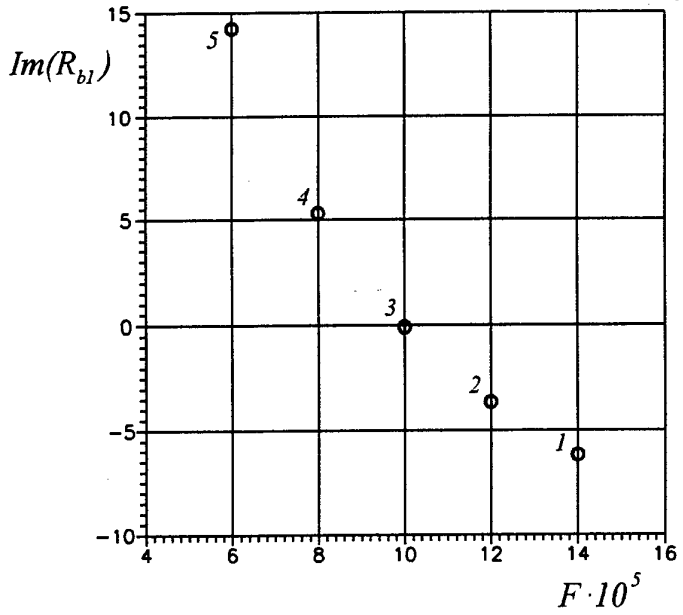


Fig. 7c Imaginary part of the first branch point as a function of disturbance frequency: $M_e = 5.95$, $T_w / T_{ad} = 0.1$.

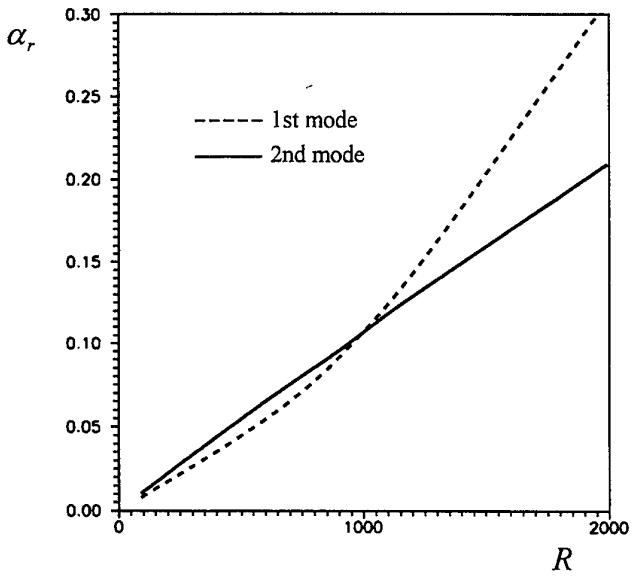


Fig. 8a Disturbance spectrum: $M_e = 6.8$, $T_w / T_{ad} = 1$, $F = 10^{-4}$; distributions $\alpha_r(R)$.

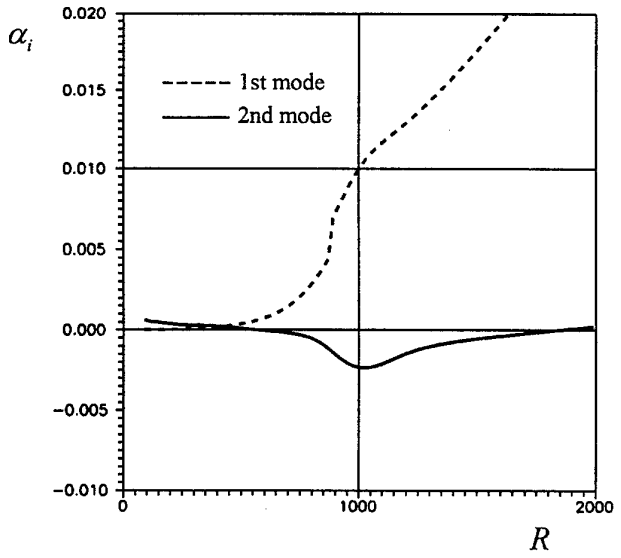


Fig. 8b Disturbance spectrum: $M_e = 6.8$, $T_w / T_{ad} = 1$, $F = 10^{-4}$; distributions $\alpha_i(R)$.

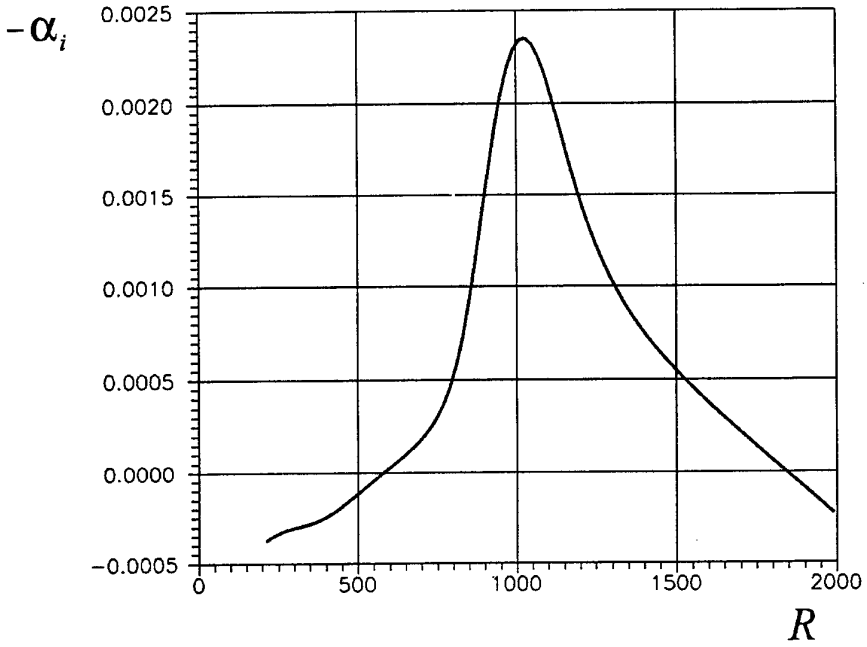


Fig. 9a Second mode increment as a function of Reynolds number; $M_e = 6.8$, $T_w / T_{ad} = 1$, $F = 10^{-4}$.

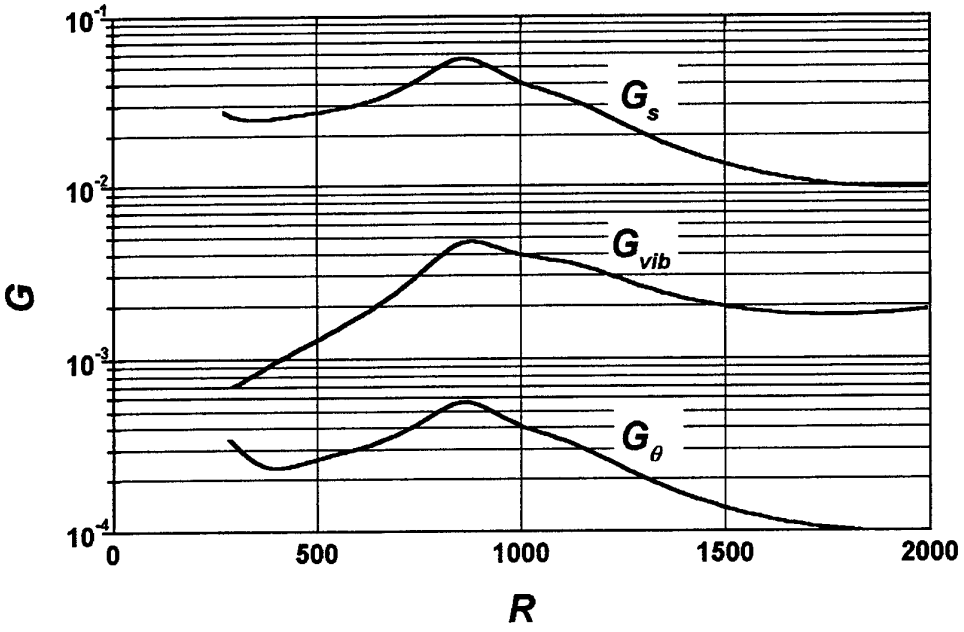


Fig. 9b Receptivity functions at $M_e = 6.8$, $T_w / T_{ad} = 1$, $F = 10^{-4}$.

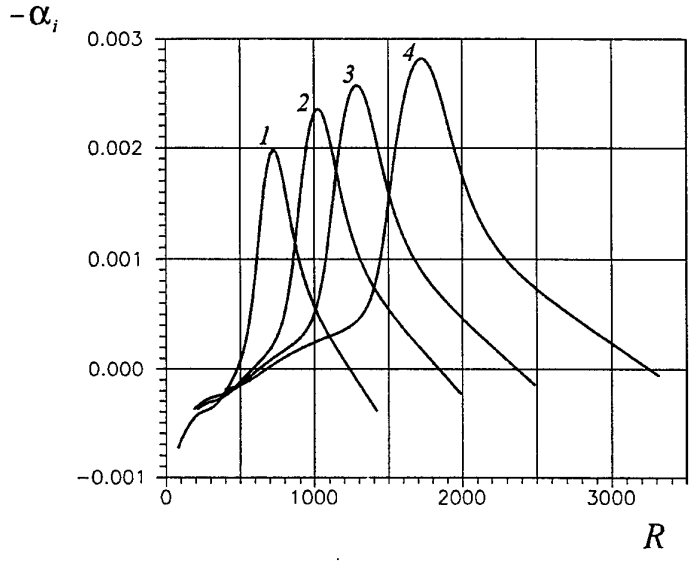


Fig. 10a Second-mode increment as a function of Reynolds number: $M_e = 6.8$, $T_w / T_{ad} = 1$; curves 1, 2, 3, and 4 correspond to the frequency parameter $F \times 10^4 = 1.4$, 1.0, 0.8 and 0.6 respectively.

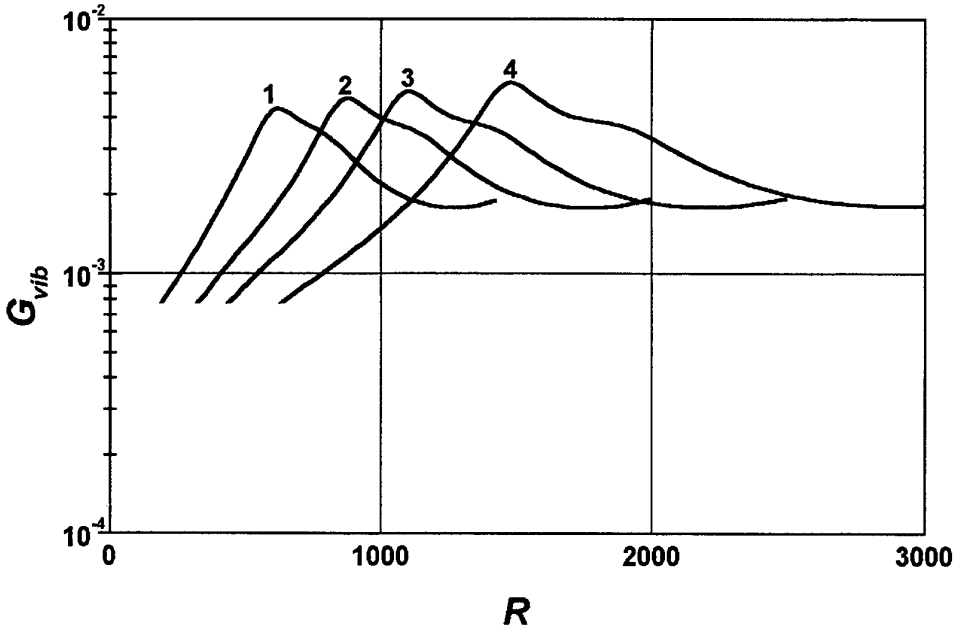


Fig. 10b Receptivity function $G_{vib}(R)$ at $M_e = 6.8$, $T_w / T_{ad} = 1$; curves 1, 2, 3, and 4 correspond to $F \times 10^4 = 1.4$, 1.0, 0.8 and 0.6 respectively.

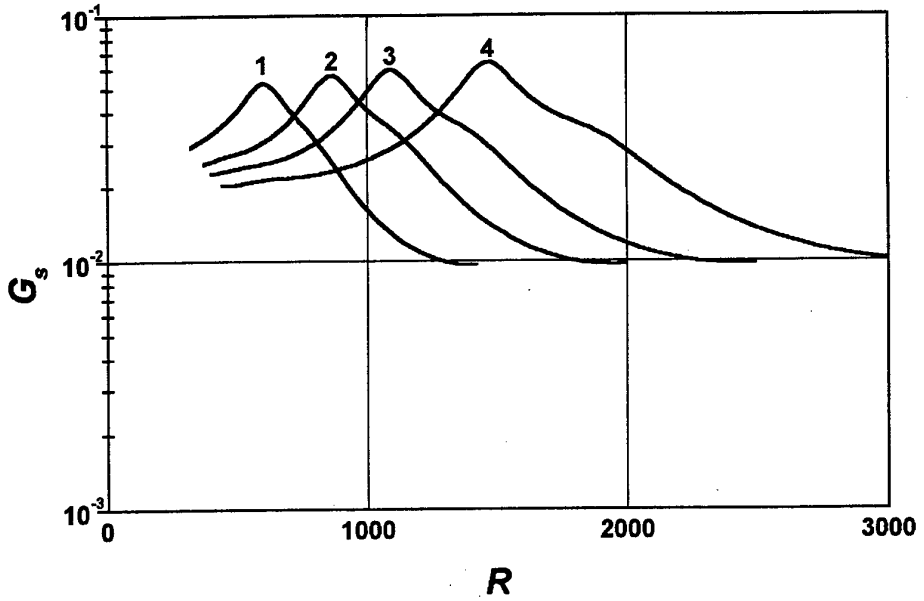


Fig. 10c Receptivity function $G_s(R)$ at $M_e = 6.8$, $T_w / T_{ad} = 1$; curves 1, 2, 3, and 4 correspond to $F \times 10^4 = 1.4$, 1.0, 0.8 and 0.6 respectively.

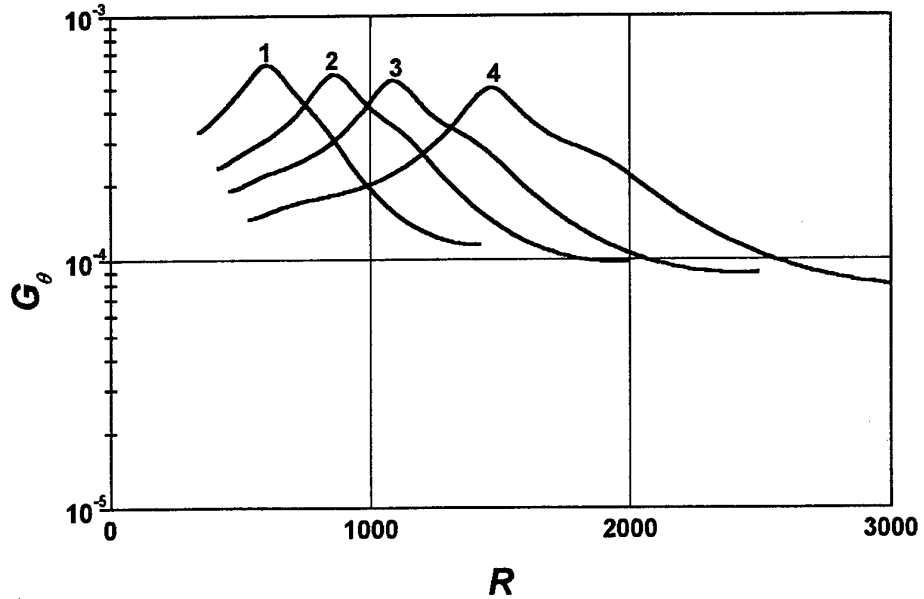


Fig. 10d Receptivity function $G_\theta(R)$ at $M_e = 6.8$, $T_w / T_{ad} = 1$: curves 1, 2, 3, and 4 correspond to $F \times 10^4 = 1.4$, 1.0, 0.8 and 0.6 respectively.

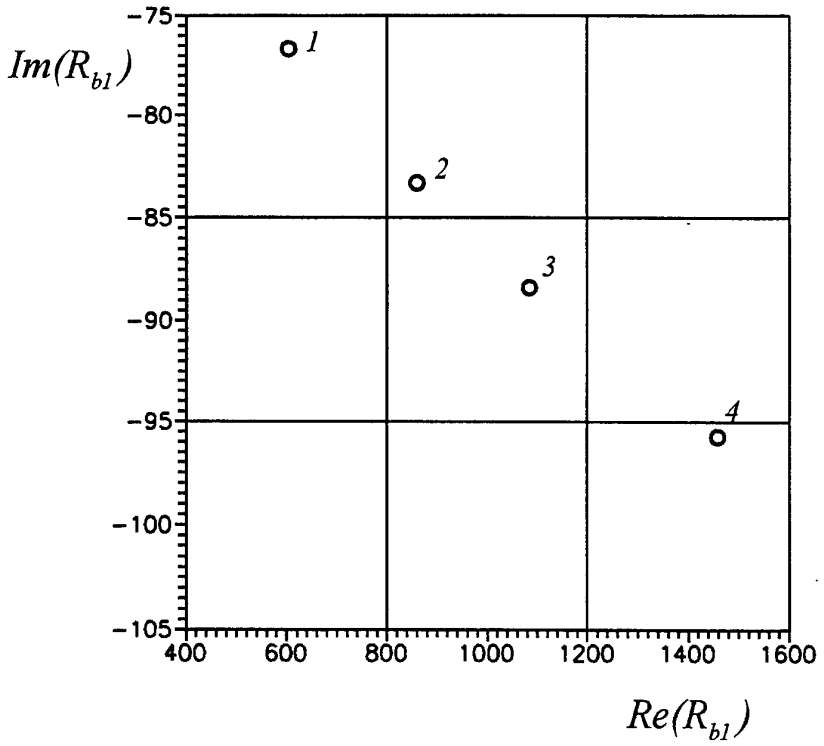


Fig. 11 Branch point locus at $M_e = 6.8$, $T_w / T_{ad} = 1$: curves 1, 2, 3, and 4 correspond to the frequency parameter $F \times 10^4 = 1.4$, 1.0, 0.8 and 0.6 respectively.

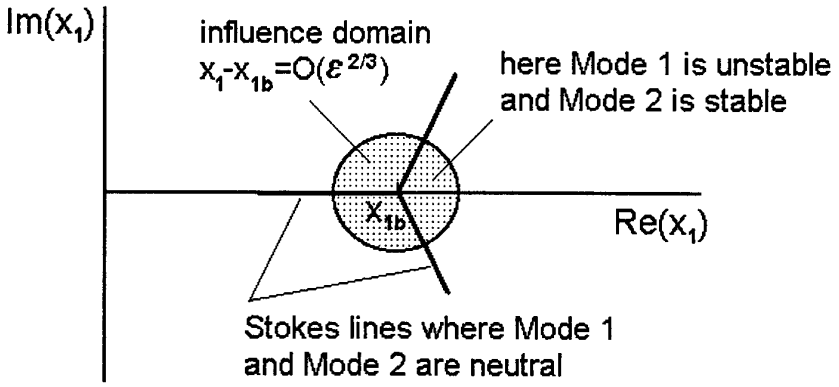


Fig. 12 Structure of the branch-point influence domain.

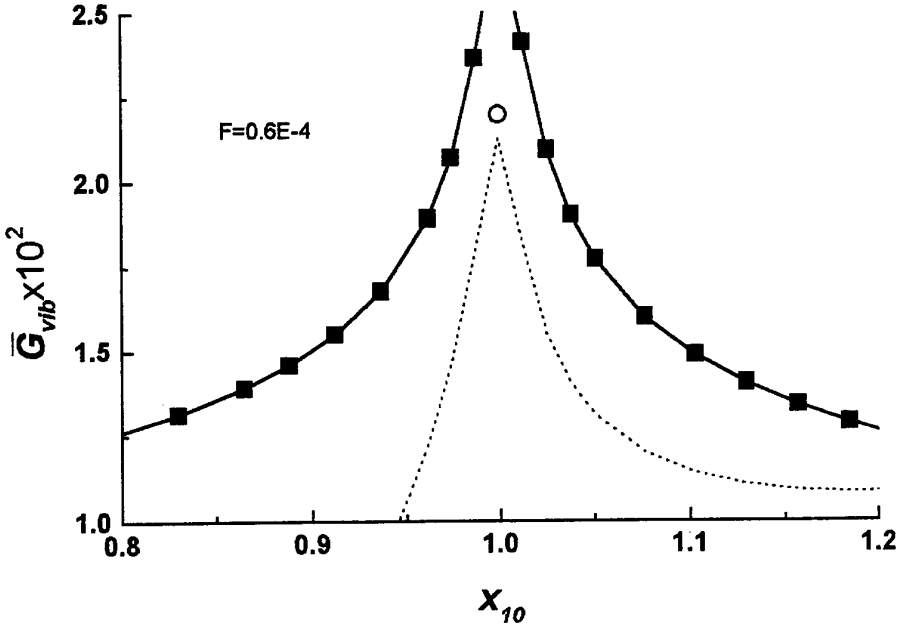


Fig. 13a Receptivity function $\overline{G}_{vib}(x_{10})$ near the branch point $x_{1b}=1$, $F=0.6\times10^{-4}$; dotted line – outer solution (3.5), solid line with square symbols – asymptotic approximation (4.36a), open circle - $\overline{G}_{vib}(x_{10}=x_{1b})$ from (4.37a).

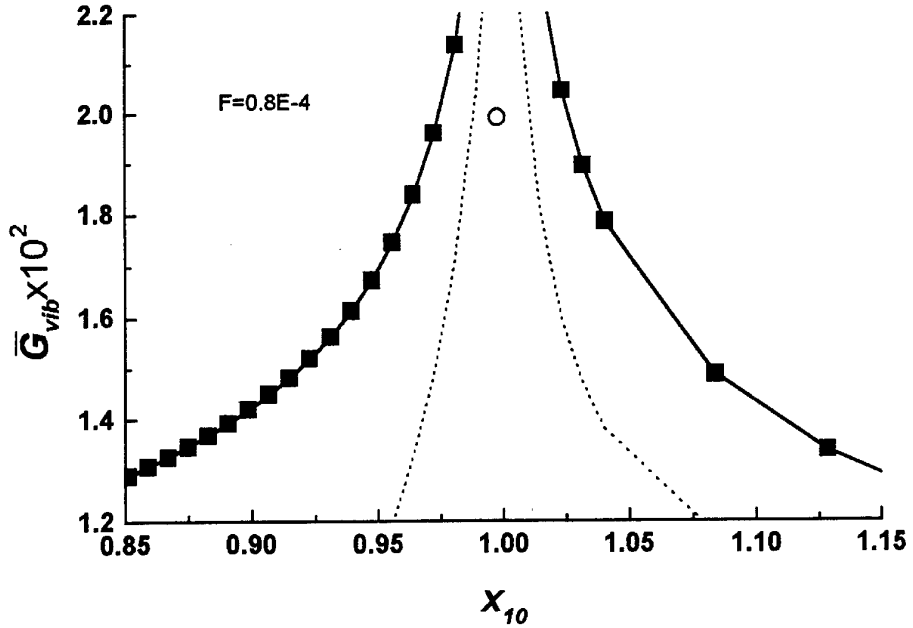


Fig. 13b Receptivity function $\overline{G}_{vib}(x_{10})$ near the branch point $x_{1b}=1$, $F=0.8\times10^{-4}$; dotted line – outer solution (3.5), solid line with square symbols – asymptotic approximation (4.36a), open circle - $\overline{G}_{vib}(x_{10}=x_{1b})$ from (4.37a).

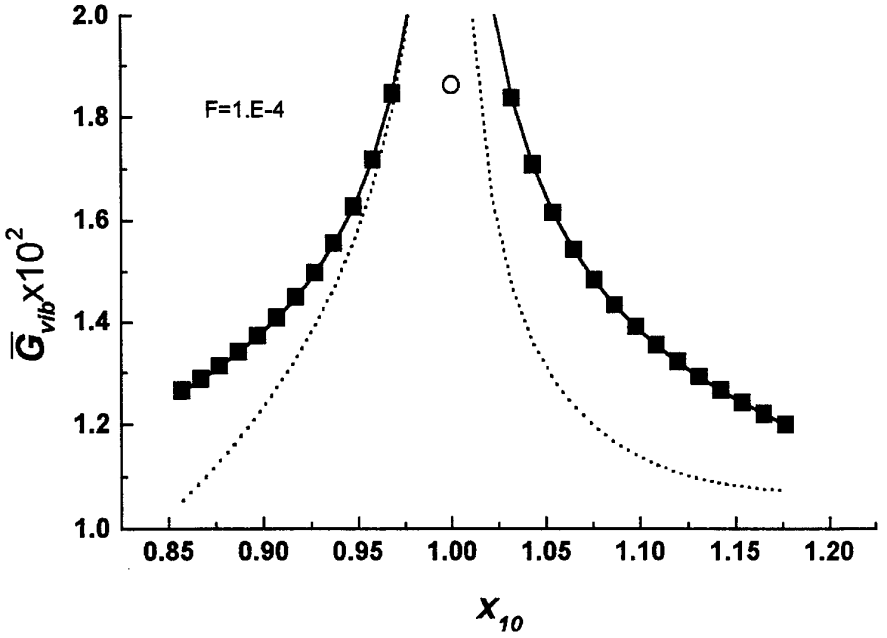


Fig. 13c Receptivity function $\overline{G}_{vib}(x_{10})$ near the branch point $x_{1b}=1$, $F=10^{-4}$; dotted line – outer solution (3.5), solid line with square symbols – asymptotic approximation (4.36a), open circle - $\overline{G}_{vib}(x_{10}=x_{1b})$ from (4.37a).

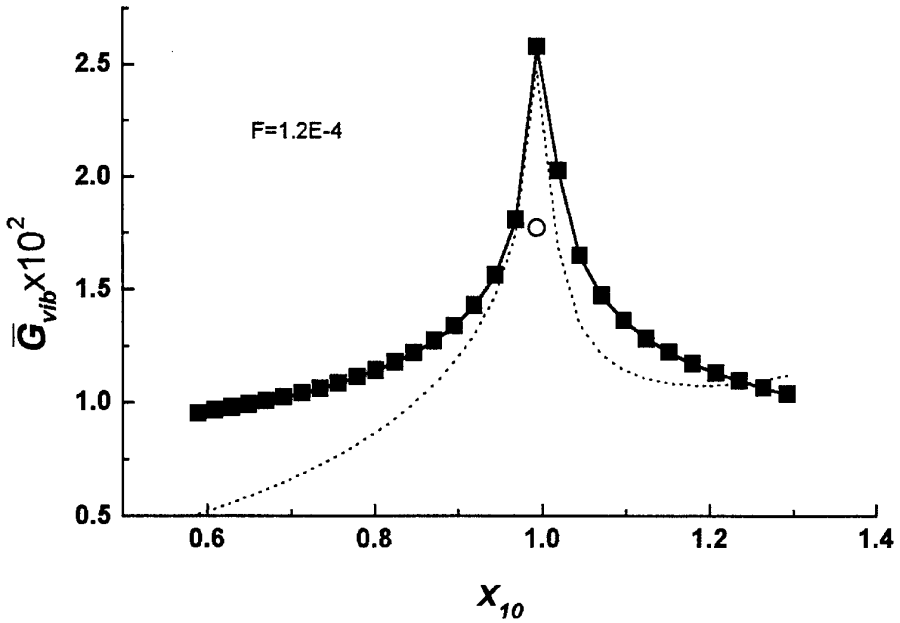


Fig. 13d Receptivity function $\overline{G}_{vib}(x_{10})$ near the branch point $x_{1b}=1$, $F=1.2\times10^{-4}$; dotted line – outer solution (3.5), solid line with square symbols – asymptotic approximation (4.36a), open circle - $\overline{G}_{vib}(x_{10}=x_{1b})$ from (4.37a).

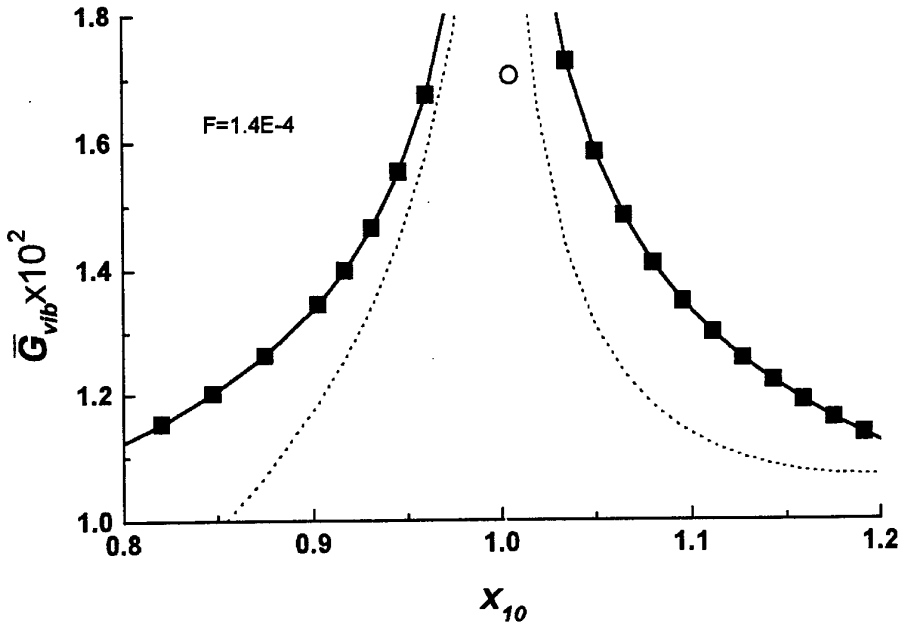


Fig. 13e Receptivity function $\overline{G}_{vib}(x_{10})$ near the branch point $x_{1b}=1$, $F=1.4\times10^{-4}$; dotted line – outer solution (3.5), solid line with square symbols – asymptotic approximation (4.36a), open circle - $\overline{G}_{vib}(x_{10}=x_{1b})$ from (4.37a).

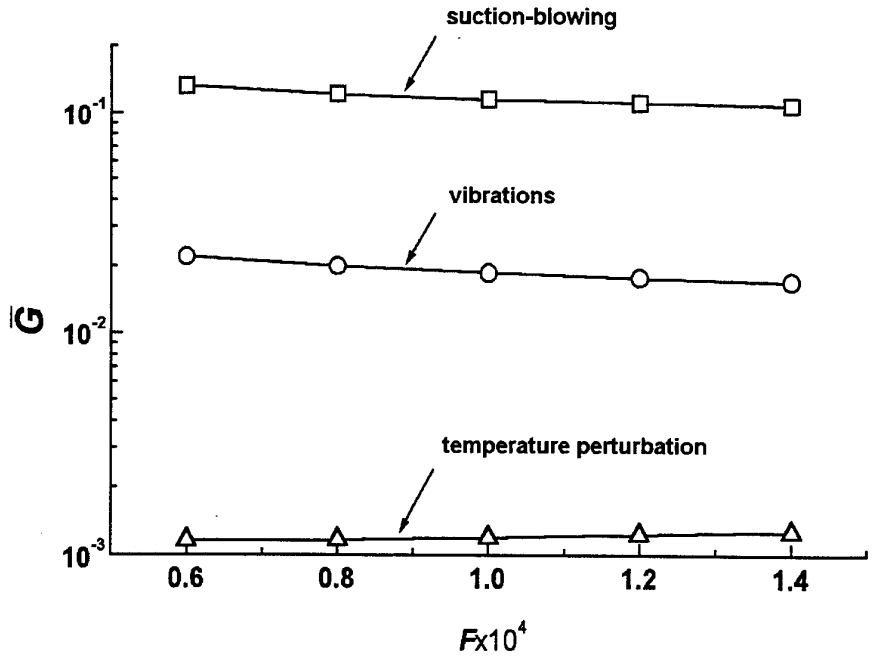


Fig. 14 Receptivity maximum $\overline{G}(x_{10} = x_{1b})$ versus frequency parameter.

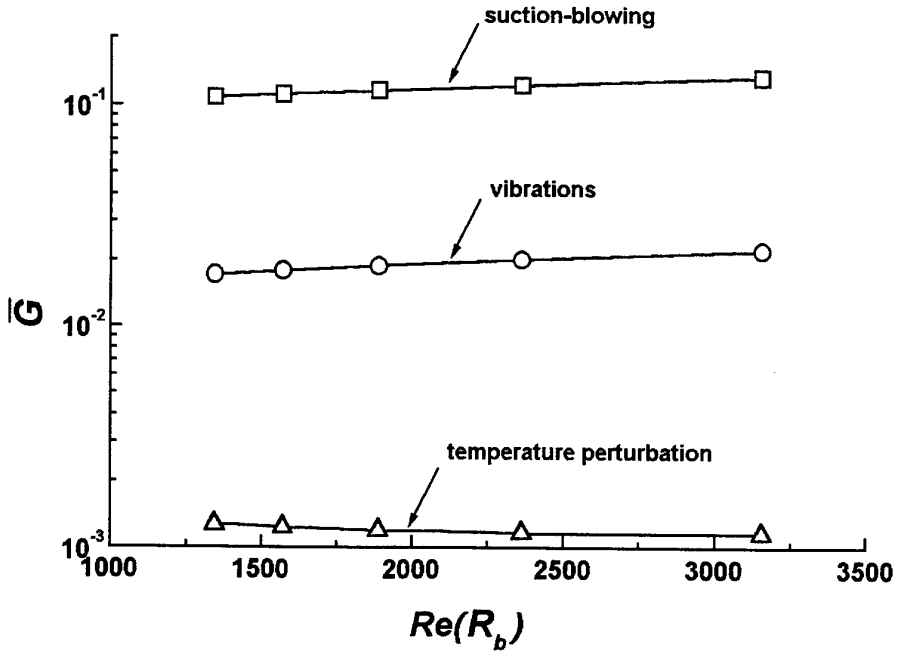


Fig. 15 Receptivity maximum $\overline{G}(x_{10} = x_{1b})$ versus the branch-point locus $\mathrm{Re}(R_b)$.

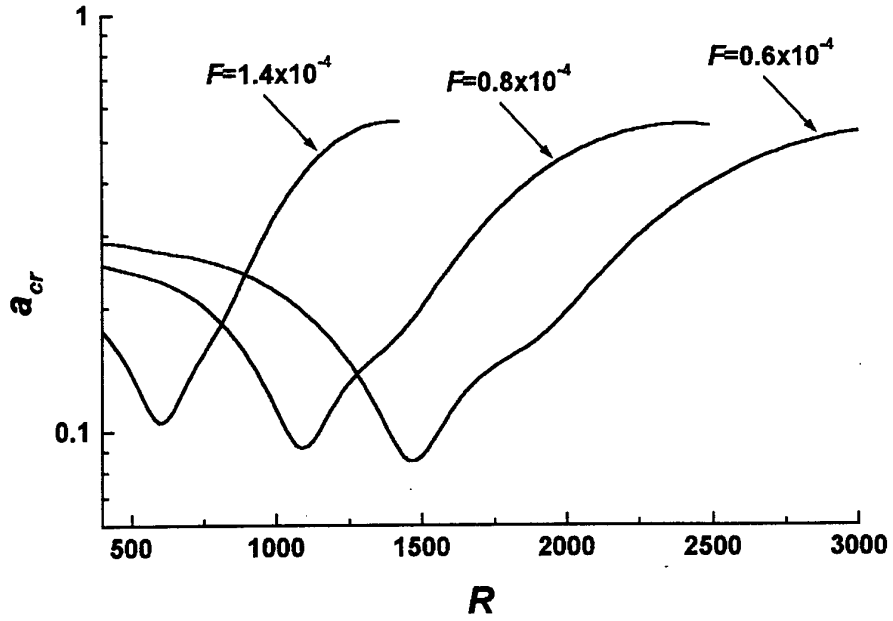


Fig. 16 Critical amplitude of local vibrations: $M_e = 6.8$, $T_w / T_{ad} = 1$.

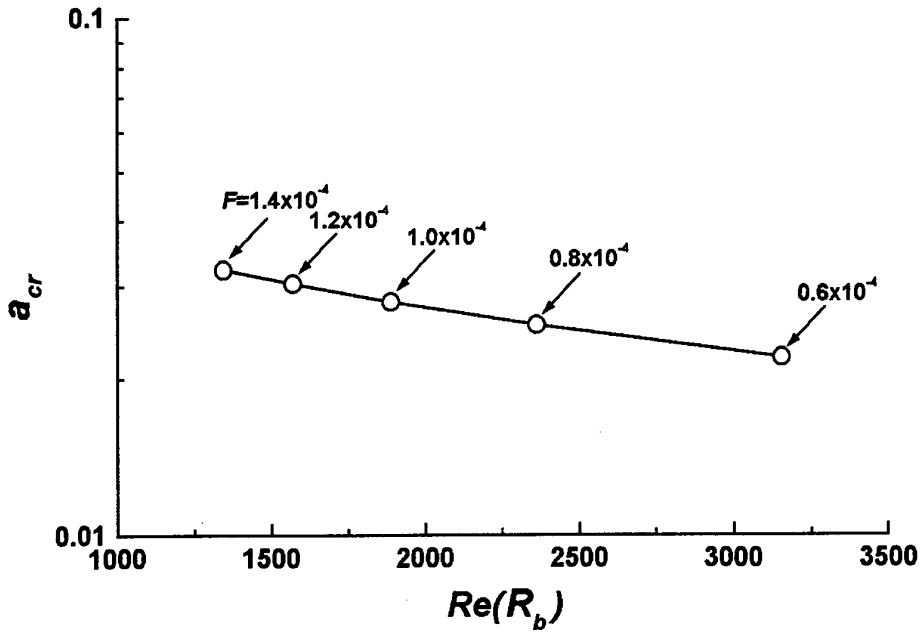


Fig. 17 Critical amplitude of local vibrations near the branch point:
$M_e = 5.95$, $T_w / T_{ad} = 0.1$.

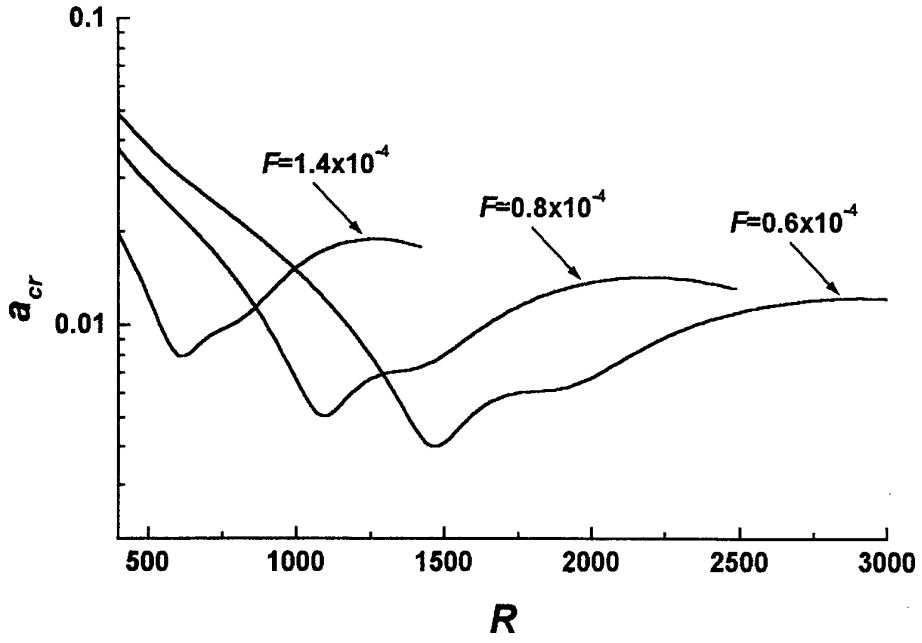


Fig. 18 Critical amplitude of distributed vibrations: $M_e = 6.8$, $T_w / T_{ad} = 1$.

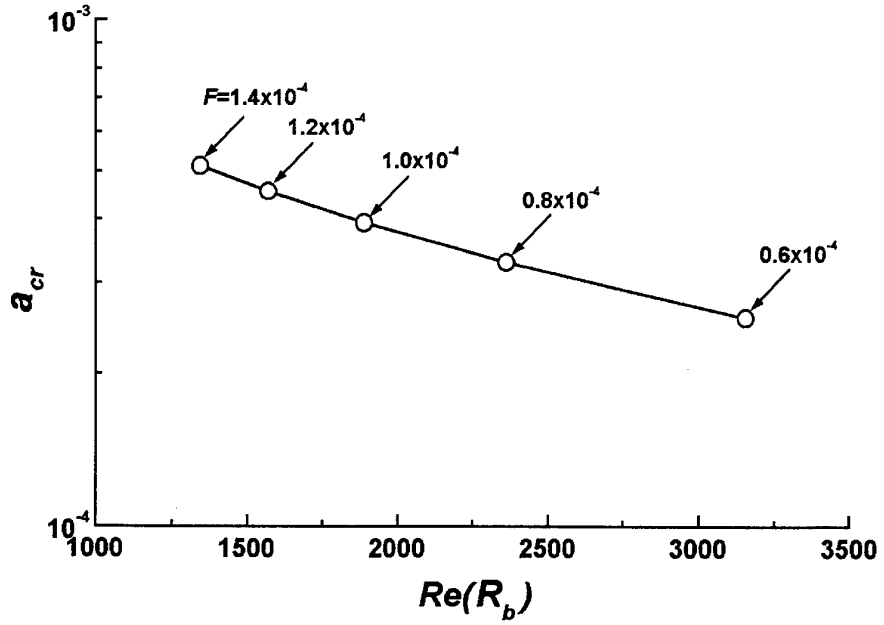


Fig. 19 Critical amplitude of distributed vibrations near the branch point: $M_e = 5.95$, $T_w / T_{ad} = 0.1$.